4

Results and Discussion

The process of neurodegeneration is based on continuous dysfunction of nerve structures and neuronal loss, progressively causing a detrimental effect on cognitive and motor-related abilities, such as memory, learning, decision making, balance, movement, talking, breathing and heart function (Silva *et al.,* 2020). Among the various age-related diseases, prevalence of chronic neurodegeneration has increasingly grown over the last few decades, It is one of the most current urgent health concerns in the society (Grodzick and Dziendzikowska, 2020). Cholinergic neurotransmitters play a very significant role in memory, learning, attention and behavior. Most importantly two enzymes, namely, Acetylcholinesterase (AChE) and Butyrylcholinesterase (BChE) are involved in the hydrolysis of acetylcholine in the brain (Nordberg *et al.,* 2013).

Plant-derived bioactive compounds (phytochemicals) have been highlighted as great therapeutic options for their preventive and biological potential in several human disorders (Fierascu *et al.,* 2020). In the human brain, phytochemicals show this therapeutic profile by exerting antioxidant and anti-inflammatory activities, as well as different protective mechanisms which make them potentially useful in counteracting neurodegeneration (Albonici *et al.,* 2020). Flavonoids are an important class of natural phytonutrients and are well known for their protective effects against neurodegeneration and neuroinflammation (Muchoney *et al.,* 2023). Oxidative stress and inflammation play a major role in brain aging and neurodegenerative diseases (Subash *et al.,* 2014). The imbalance of antioxidants with reactive oxygen species results in excessive oxidative stress, which causes a series of biochemical and pathological reactions which eventually lead to an extensive neuronal degeneration (Li *et al.,* 2022). Thus, antioxidants have potential therapeutic properties to overcome neurodegenerative diseases. Flavonoids, both from food and medicinal plants, are naturally occurring polyphenols with various pharmacological activities, such as reactive oxygen species scavenging activitiy, anticancer activity and anti-inflammatory effects. Thus, these natural flavonoids are commonly recognized as one of the most promising sources of antioxidants with high safety and effectiveness (Li *et al*., 2022).

With the above aspects in view, the present study entitled '**Neuroprotective effect of synthesized zinc oxide nanoparticle-capped catechin'** focused on studying the *in vitro* neuroprotective activity of synthesized zinc oxide nanoparticle-capped catechin from *Camellia sinensis*.

The work consisted of five phases - Phase I dealt with Evaluation of active compounds against neuroprotective target proteins using molecular docking studies, Phase II involved characterization of the selected medicinal plant *Camellia sinensis* - preliminary phytochemical studies and antioxidant activities and identifications of a novel compound using chromatographic and spectral studies, Phase III dealt with synthesis of zinc oxide nanoparticles from *Camellia sinensis* and its characterization, Phase IV included characterization of synthesized zinc oxide nanoparticle-capped catechin and evaluation of its *in vitro* neuroprotective activity, Phase V had the assessment of *in vitro* neuroprotective activity of synthesized zinc oxide nanoparticle-capped catechin to neuroblastoma cell line (neuro 2a cells)

Results of the study are furnished and discussed under the following headings,

4.1. Phase I: Evaluation of active compounds against neuroprotective target proteins using molecular docking studies

4.1.1. Molecular docking using commercial drugs and natural compounds

4.1.1.1 Prediction of ADMET properties of commercial drugs and natural compounds

4.1.1.2. Analysis of ADMET properties of commercial drugs

4.1.1.3. Analysis of ADMET properties of natural compounds

4.1.1.4. Protein preparation

4.1.1.5. Docking score of neuroprotective target proteins with ligands

4.1.1.6. Molecular docking of ligands to protein acetylcholinesterase (AChE) active site

4.2 Phase II: Characterization of *Camellia sinensis* and identification of its bioactive compound

4.2.1. Qualitative screening for phytoconstituents in *Camellia sinensis*

4.2.2 Quantification of phytochemical constituents in *Camellia sinensis*

4.2.2.1. Total phenol content

4.2.2.2. Total flavonoid content

4.2.3. Antioxidant Radical Scavenging Activity

4.2.3.1. Diphenyl-Picryl Hydrazine (DPPH) radical scavenging activity in *Camellia sinensis*

4.2.3.2. Ferric Reducing Antioxidant Power (FRAP) radical scavenging activity in *Camellia sinensis*

4.2.3.3. Total Antioxidant Capacity (TAC) in *Camellia sinensis*

4.2.4. Enzymatic antioxidants in ***Camellia sinensis***

4.2.5. Non-Enzymatic antioxidants activity in *Camellia sinensis*

4.2.6. Active constituent in *Camellia sinensis*

4.2.6.1. Results of column chromatography analysis of *Camellia sinensis* extract

4.2.6.2. Results of HPTLC analyses of selected chromatographic fraction of *Camellia sinensis* extract

4.2.6.3. Results of ultraviolet–visible spectroscopy analysis of selected chromatographic fraction of *Camellia sinensis*

4.2.6.4. Catechin content in *Camillia sinesis*

4.2.6.5. Results of FT-IR spectroscopy of the selected chromatographic fraction of *Camellia sinensis* extract

4.2.6.6. Results of GC-MS analysis of chromatographic fraction of *Camellia sinensis* extract

4.2.6.7. Results of NMR of the selected chromatographic fraction of *Camellia sinensis* extract

4.2.6.8. Results of LC-MS of the selected chromatographic fraction of *Camellia sinensis* extract

4.3. Phase III: Characterization of synthesized zinc oxide nanoparticles from *Camellia sinensis*

4.3.1. Characterization of synthesized zinc oxide nanoparticles from *Camellia sinensis*

4.3.1.1. Visual observation of synthesized zinc oxide nanoparticles

4.3.1.2. Ultra Visible spectrum of synthesized zinc oxide nanoparticles

4.3.1.3. Surface topography of analysis synthesized zinc oxide nanoparticles from *Camellia sinensis* using Scanning Electron Microscopy (SEM)

4.3.1.4. Elemental mapping analysis of synthesized zinc oxide nanoparticles from *Camellia sinensis*

4.3.1.5. Results of X-ray diffraction studies of the synthesized zinc oxide nanoparticles from *Camellia sinensis*

4.3.1.6. Functional group analysis of the synthesized zinc oxide nanoparticles from *Camellia sinensis* using Fourier Transform Infra-Red (FTIR) spectroscopy

4.3.1.7. Surface Charge of the synthesized zinc oxide nanoparticles from *Camellia sinensis* using zeta potential

4.3.2. Antioxidant activity of synthesized zinc oxide nanoparticles from *Camellia sinensis*

4.3.3. Neuroprotective effect of synthesized zinc oxide nanoparticles from *Camellia sinensis*

4.3.3.1. Results of Thin Layer Chromatography (TLC) with bioassay detection for AChE inhibition

4.3.3.2. Acetyl cholinesterase (AChE) inhibitory activity of synthesized zinc oxide nanoparticles from *Camellia sinensis*

4.4. Phase IV: Synthesized zinc oxide nanoparticle-capped catechin their characterization and *in vitro* neuroprotective activity

4.4.1. Characterization of synthesized zinc oxide nanoparticle-capped catechin

4.4.1.1. Results of UV – visible spectrum analysis of synthesized zinc oxide nanoparticle-capped catechin

4.4.1.2. Results of surfaces topography analysis of synthesized zinc oxide nanoparticle-capped catechin by SEM

4.4.1.3. Analysis of diffractogram of synthesized zinc oxide nanoparticle-capped catechin

4.4.1.4. FTIR spectrum analysis of synthesized zinc oxide nanoparticle-capped catechin

4.4.1.5. Results of zeta potential studies on the synthesized zinc oxide nanoparticle-capped catechin

4.4.2. Antioxidant activity of synthesized zinc oxide nanoparticle-capped catechin

4.4.3. *In vitro* neuroprotective activity of synthesized zinc oxide nanoparticle-capped catechin

4.4.3.1. Entrapment efficiency and loading capacity of synthesized zinc oxide nanoparticle-capped catechin

4.4.3.2. Results of *In vitro* release study of synthesized zinc oxide nanoparticle-capped catechin

4.4.3.3. Results of Acetylcholinestrase inhibition by TLC

4.4.3.4. Acetylcholinestrase inhibition activity of synthesized zinc oxide nanoparticle-capped catechin

4.5. Phase V: Assessment *in vitro* neuroprotective activity of synthesized zinc oxide nanoparticle-capped catechin to neuro 2a cells

4.5.1. Results of Cell viability of neuro 2a cells using the synthesized zinc oxide nanoparticle-capped catechin

4.5.2. Results of Lactate Dehydrogenase (LDH) leakage of synthesized zinc oxide nanoparticle-capped catechin

4.5.3. Analysis of morphological changes in neuro 2a cell lines on treatment with synthesized zinc oxide nanoparticle-capped catechin

4.5.4. Results of superoxide dismutase activity of synthesized zinc oxide nanoparticle-capped catechin

4.5.5.. Results of DCFDA (DiChlorodihydro Fluorescein DiAcetate) staining of synthesized zinc oxide nanoparticle-capped catechin

4.5.6. Results of Acetylcholinestrase activity of synthesized zinc oxide nanoparticle-capped catechin

4.5.7. Results of cell cycle analyses by flow cytometer of synthesized zinc oxide nanoparticle-capped catechin

4.1. Phase I

Evaluation of active compounds against neuroprotective target proteins using molecular docking studies

Molecular docking is the most widely used computational structure-based drug design technique. It was designed to operate between a tiny molecule (ligand) and a macromolecule target (protein). Molecular docking has a wide range of uses in drug discovery, including structure-activity investigations, lead optimization and virtual screening for new leads (Stanzione *et al.*, 2021).

4.1.1. Molecular docking using commercial drugs and natural compounds

The current research was carried out in order to predict Absorption, Distribution, Metabolism, Excretion and Toxicity commonly (ADMET) properties of natural phyto constituents such as cyanidin, catechin, kaemopferol, genistein, epicatechin, quarcetin 3-o-glucoside, epicatechin gallate, rutin, hesperetin, theaflavin-3-o-gallate, apigenin, zinc, herperetin, kemopferol-3-o-rutinoside, quercetin, thea flavin-3'-gallate, theaflavin, gallic

acid, caffine, kaempferide 3-glucoside and commercial drugs (galanthamine, rivastigmine, tacrine, memantine and donepezil) to analyse their interaction with neuroprotective targets through docking studies.

4.1.1.1. Prediction of ADMET properties of commercial drugs and natural compounds

Absorption, Distribution, Metabolism, Excretion and Toxicity commonly known as ADMET, is the key criteria for sorting ligands in drug discovery programs. It serves as a primary testing requirement for any candidate molecule. A numbers of softwares are available for predicting and analyzing ADMET properties. The most important / widely used software / programs include ADMET parameter predictors, metabolic fate predictors, metabolic stability predictors, cytochrome P450 substrate predictors and physiology based pharmacokinetic modelling software (Pan *et al.,* 2022).

ADMET properties of commercial drugs and natural compounds were analysed using the PKCSM software (https://biosig.lab.uq.edu.au/pkcsm). The results are provided in Table III. First, a prospective therapeutic molecule is chosen by ADMET screening, which aids in forecasting the compounds behaviour using *in silico* modelling. The docking analysis describes the drug-like activity of the ligand molecule by applying ADMET properties. A software for ADMET prediction has been utilized to help optimize a given molecule and increase its desired properties.

Table III illustrates the ADMET properties of commercial drugs (galanthamine, rivastigmine, tacrine, memantine and donepezil) and the natural compounds (cyanidin, catechin, kaemopferol, genistein, epicatechin, quarcetin 3-o-glucoside, epicatechin gallate, rutin, hesperetin, theaflavin-3-o-gallate, apigenin, zinc, herperetin, kemopferol-3-o-rutinoside, quercetin, thea flavin-3'-gallate, theaflavin, gallic acid, caffine and kaempferide 3-glucoside).

Table III

ADMET properties of commercial drugs and natural compounds

S.No	Commercial drugs and Natural compounds	Pub Chem ID	Chemical structure	No. of donor H bond	No. of acceptor H bond	Molecular mass	Human oral absorption	Log P	Blood-Brain Barrier permeability
Commercial drugs									
1.	Galanthamine	9651	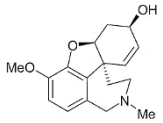	1	4	287.359	94.994	1.8503	-0.081
2.	Rivastigmine	77991	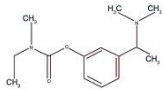	1	1	250.34	95.866	2.6941	0.234
3.	Tacrine	1935	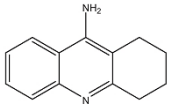	1	2	198.269	95.399	2.6958	0.316
4.	Memantine	4054	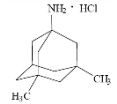	1	1	179.307	91.234	2.6941	0.603
5.	Donepezil	3152	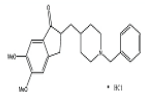	0	4	379.5	93.707	4.3611	0.157

S.No	Commercial drugs and Natural compounds	Pub Chem ID	Chemical structure	No. of donor H bond	No. of acceptor H bond	Molecular mass	Human oral absorption	Log P	Blood-Brain Barrier permeability
Natural compounds									
6.	Cyanidin	128861	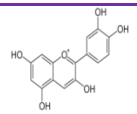	5	6	287.247	87.303	2.9089	-1.243
7.	Catechin	9064	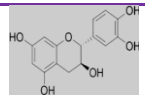	5	5	290.271	68.829	1.5461	-1.054
8.	Kaemopferol	5280863	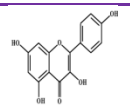	5	6	290.24	74.29	1.5461	-0.939
9.	Genistein	5280961	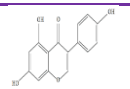	4	6	1.546	93.387	2.2824	-0.71
10.	Epicatechin	72276	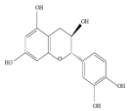	3	5	2.9089	68.829	2.5768	-1.054
11.	Quarcetin 3-o-glucoside	5484066	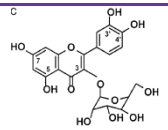	5	6	290.271	47.999	1.5461	-1.688

S.No	Commercial drugs and Natural compounds	Pub Chem ID	Chemical structure	No. of donor H bond	No. of acceptor H bond	Molecular mass	Human oral absorption	Log P	Blood-Brain Barrier permeability
12.	Epicatechin gallate	107905	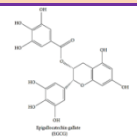	8	12	464.379	62.096	-0.5389	-1.847
13.	Rutin	5280805	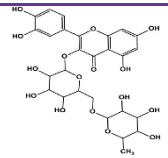	7	10	442.376	23.446	2.5276	-1.899
14.	Hesperetin	107905	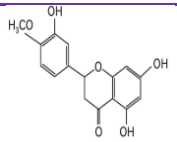	10	16	610.521	70.277	-1.6871	-0.719
15.	Thea flavin-3-o-gallate	136825044	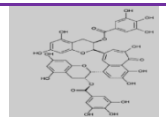	3	6	302.282	43.318	2.5185	-2.566
16.	Apigenin	5280443	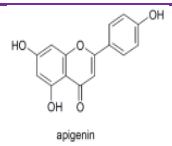	11	16	716.604	93.25	3.1949	-0.734

S.No	Commercial drugs and Natural compounds	Pub Chem ID	Chemical structure	No. of donor H bond	No. of acceptor H bond	Molecular mass	Human oral absorption	Log P	Blood-Brain Barrier permeability
17.	Zinc	23994	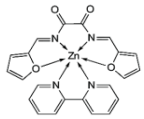	3	5	270.24	100	2.5768	0.026
18.	Herperetin	3115	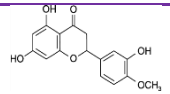	0	0	65.39	70.277	-0.0025	-0.719
19.	Kemopferol-3-o-rutinoside	5318767	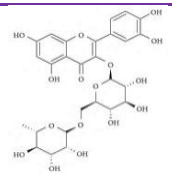	3	6	302.282	30.743	2.5185	-1.669
20.	Quercetin	5280343	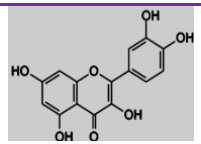	9	15	594.522	77.207	-1.3927	-1.098
21.	Thea flavin-3'-gallate	136825044	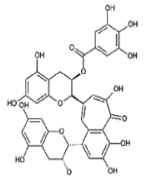	5	7	302.238	50.555	1.988	-2.092

S.No	Commercial drugs and Natural compounds	Pub Chem ID	Chemical structure	No. of donor H bond	No. of acceptor H bond	Molecular mass	Human oral absorption	Log P	Blood-Brain Barrier permeability
22.	Theaflavin	135403798	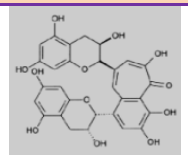	10	15	704.637	65.009	3.4386	-1.577
23.	Gallic Acid	370	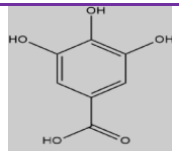	9	12	564.499	43.374	2.2134	-1.102
24.	Caffine	2519	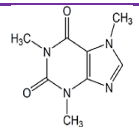	4	4	170.12	99.272	0.5016	-0.268
25.	Kaempferide 3-glucoside	44259083	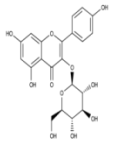	0	6	194.194	48	-1.0293	-1.514

Chemical structure: Two dimensional structures of natural compounds and commercial drugs
No. of Donor H bond: Number of hydrogen bond donors (Range: 0.0-12.0)
No. of acceptor H bond: Number of hydrogen bond acceptors (Range: 2.0-20.0)
Molecular mass: Molecular weight of the molecule (Range: 130.0-725.0)
Human oral absorption: Predicted Human oral absorption (Range: 30.0-110.0)
Log P: Predicted octanol/water partition coefficient (Range: -2.0-6.5)
Blood-Brain Barrier permeability: Predicted brain/blood partition coefficient (Range from -3.0 to 1.2)

4.1.1.2. Analysis of ADMET properties of commercial drugs

It is evident from the table that elevated intestinal absorption in humans suggests that the compounds of interest could be more readily absorbed by the digestive system when taken orally. The penetration through the Blood-Brain Barrier is computed to be the best for rivastigmine and almost similar to tacrine and donepezil and comparatively higher than other commercial drugs. It was discovered that galanthamine had a log P value of 1.8503 and four H bond acceptors. It is revealed that rivastigmine has a log P value of 2.6941 and one H bond acceptors. It can also be noticed that tacrine, a commercial medication, has two H bond acceptors and a log P value of 2.6958. It is shown that memantine has a log P value of 2.6941 and one H bond acceptor. It is discovered that donepezil has a log P value of 4.361 and four H bond acceptors. Hence, the findings demonstrate that commercial medications, which serve as reference pharmaceuticals for the natural substance, were examined for their ADMET qualities, including galanthamine, rivastigmine, tacrine, memantine and donepezil. The medications donepezil and galanthamine, which are two of the five commercially available pharmaceuticals, have the highest number of acceptor H bonds four, to be exact.

4.1.1.3. Analysis of ADMET properties of natural compounds

From the table, it can be clearly stated that the ADMET properties of cyanidin have six acceptor H bonds, with a log P of 2.9089. It is discovered that catechin has a log P value of 1.5461 and five acceptor H bonds. Six acceptor H bonds were identified in kaempferol and its log P value is 1.5461. The H bond acceptor count for genistein was found to be six and with a log P value of 2.2824. It is obvious that (−)-epicatechin has a log P of 2.2824 and six acceptors H bonds. Quarcetin 3-o-glucoside is a naturally occurring chemical with a log P value of 2.5768 and 5 acceptor H bonds. It was noticed that the naturally occurring molecule epicatechingallate has 12 acceptor H bonds and a log P value of 0.5389. It was also shown that rutin has a log P value of 2.5276 and five acceptor H bonds. The natural chemical hesperetin has a log P value of 1.6871 and 16 acceptor H bonds. It is revealed that apigenin has a log P value of 3.1949 and 12 acceptor H bonds. It can be stated that the zinc has five acceptor H bonds, with a log P of 2.5768. It is revealed that the natural chemical hesperidin has a log P value of -0.0025 and 0 acceptors H bonds. It is also shown that the natural chemical kaempferol-3-O-rutinoside has six acceptor H bonds and a log P of 2.5185. It is discovered that the naturally occurring chemical quercetin has 15 acceptor H bonds and a log P value of 1.3927. Log P has 3.4386, 2.5185 and 1.988 for the natural compounds

theaflavins, theaflavin-3-o-gallate and theaflavin-3-gallate respectively. The compounds have 15, 6, and 7 acceptors H bonds. It can be noticed that gallic acid has 12 acceptor H bonds with log P value of 2.2134. Caffeine, a naturally occurring molecule, has four acceptor H bonds with a log P value of 0.5016 and the naturally occurring molecule kaempferide 3-glucoside has six acceptor H bonds and a log P value of -1.0293.

Hence the results show that the natural compounds such as cyanidin, catechin, kaemopferol, genistein, epicatechin, quarcetin 3-o-glucoside, epicatechin gallate, rutin, hesperetin, thea flavin-3-o-gallate, apigenin, zinc, herperetin, kemopferol-3-o-rutinoside, quercetin, thea flavin-3'-gallate, theaflavin, gallic acid, caffine, kaempferide 3-glucoside Among those 15 natural compounds, both herperetin and apigenin has more acceptor H bond (16) compared with other compound and followed theaflavin, quercetin has (15) acceptor H bond compared with other natural compounds based on the chemical structure according to the Table 3.

Thus it is evident from Table III ADMET characteristics of catechin that its oral bioavailability (less than 70 %) was found to be 68.82 as predicted by LD 50 value. ADMET did not pose a risk for hepatotoxicity. Catechin has the lowest amount of toxicity among possible ligands based on several pharmacological characteristics. It is well established that the characteristics of catechin and epicatechin-3-gallate affect bioavailability, cell penetration and metabolism. Nearly all expected features of the tested molecule satisfied the Lipinski's rule of five and fell inside the range predicted by QikProp for 62.094 and 68.829 % of known oral medicines, respectively. Lipinski's Rule of Five indicated that both commercial drugs (rivastigmine) and natural substances (catechin) showed signs of drug-likeness. Ligands may be employed in subsequent studies to aid in the development of potential medications.

The results are related to the previously mentioned findings Natarajan *et al*., (2015) who reported that the compound with the properties of cyclopentadeca-4, 12-dienone ADMET (4Z, 12Z) can be considered the greatest hit molecule and might potentially be turned into a potent antidiabetic drug. The above findings are supported by Ahmad *et al*., (2024) who emphasized in his studies that the ADMET analysis of the 50 marine-origin compounds showed 30 of them to follow Lipinski's rule of five. These 30 compounds were docked with multiple target proteins involved in neurodegenerative

disorders. Another study by Ganesh and Kannaniyanar, (2017) had reported that, *Ginkgo biloba* (Maidenhair tree) contains a phytochemical called -5,15,18-trione, which binds to tau protein kinase, beta secretase and cholinesterase pharmacological targets very well, according to docking investigations.

Thus, it is evident from the current findings that the ADMET properties of the compounds studied all the compounds have drug-like properties.

4.1.1.4. Protein preparation

Prior to docking, it is important to identify the binding site in the target protein, information for which is available many times through the structures of the complexes of the protein with its substrate. Possible pockets in the set of sodium channel protein structures were first identified by detecting binding sites in all the proteins and then by identifying unique pockets that could serve as feasible targets for inhibitors (Meraj *et al.*, 2012).

The three dimensional (3D) structures of neuroprotective target proteins are depicted in Figure 8.

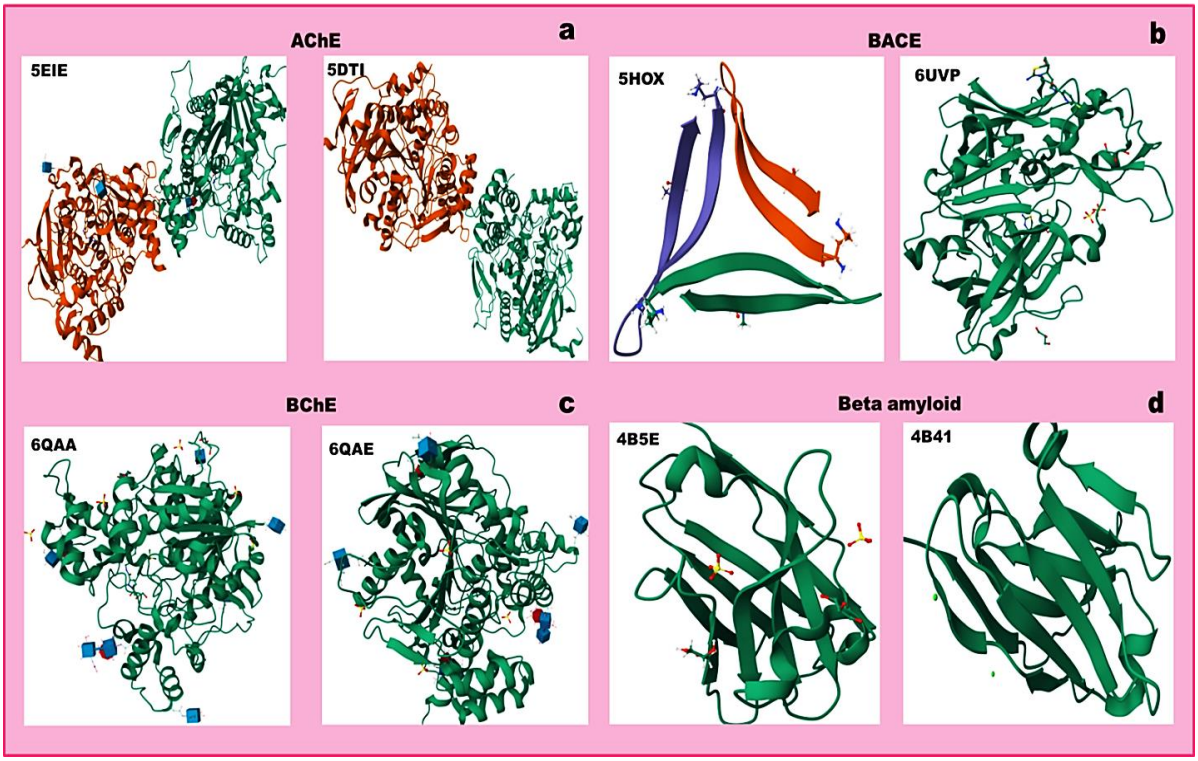

Figure 8: Complex structure of neuroprotective target proteins

a) AChE (5EIE & 5DTI**),** **b) BACE (**5HOX & 6UVP**),**
c) BChE (6QAA & 6QAE**)** and **d) Beta amyloid (**4B5E & 4B41**)**

From the figure, it is clearly understood that, the crystal structures of the neuroprotective target proteins were retrieved from the Protein Data Bank (PDB) (https://www.rcsb.org/pdb). They are acetylcholinesterase (AChE) (PDB ID: 5EIE 5DTI); butyrylcholinesterase (BChE) (PDB ID: 6QAA 6QAE); β-secretase (BACE) (PDB ID: 5HOX, 6UVP) and beta amyloid (PDB ID: 4B5E 4B41). In general, the protein structures are refined for their bond orders, formal charges and missing hydrogen atoms, topologies, incomplete and terminal amide groups. Water molecules beyond 5 A^o of the hetero atom were removed. The possible ionization states were generated for the heteroatom present in the protein structure and the most stable state was chosen. The hydrogen bonds were assigned and orientations of the retained water molecules were corrected.The structures of the ligands were generated using the Chem Draw Exchange (CDX) format using the tool Chem Draw ultra-version 8.0. These ligands were then converted to the mol 2 format and subjected to LigPrep module of Maestro in the Schrodinger suite 2013. They were optimized for their geometry, desalted and corrected for their chiralities and missing hydrogen atoms. The 2D structures were transformed into 3D structures by including stereo chemistry, ionization, tautomeric changes and energy minimization. Bond orders of these ligands were fixed and the charged groups were neutralized.

The ionization and tautomeric states were generated between pH of 6.8 to 7.2 using Epik module. In the final stage of LigPrep, compounds were minimized using Optimized Potentials for Liquid Simulations-2005 (OPLS-2005) force field in Impact package of Schrodinger until a root mean square deviation of 1.8A^o was achieved. Steepest descent algorithm was used for minimization, followed by conjugate gradient method. A single low energy ring conformation per ligand was generated and the optimized ligands were used for docking analysis. The ligand was retained in the crystal structure of the prepared protein which was used for the receptor grid construction. The binding box dimensions (within which the centroid of a docked pose is confined) of the protein was set to 14A^o x 14A^o x 14 A^o.

4.1.1.5. Docking score of neuroprotective target proteins with ligands

The docking interaction data of AChE, BACE, BChE and beta amyloid proteins are displayed in Table IV, alongwith the binding energy of neuroprotective targets with ligands.

Table IV

Docking score of neuroprotective target proteins with ligands

S.No.	Natural compounds and commercial drugs	PubChem ID	*Neuroprotective target proteins							
			AChE		BACE		BChE		Beta amyloid	
			5EIE	5DTI	5HOX	6UVP	6QAA	6QAE	4B5E	4B41
Commercial drugs										
1.	Galanthamine	9651	-5.207	-3.416	-3.543	-2.522	-2.01	-4.939	-1.409	-1.5
2.	Rivastigmine	77991	-7.104	-7.904	-2.979	-4.894	-6.829	-6.039	-2.845	-2.528
3.	Tacrine	1935	-6.825	-7.646	-2.946	-5.574	-5.215	-7.229	-2.262	-
4.	Memantine	4054	-1.37	-7.233	-3.543	-6.475	-7.532	-8.40	-3.74	-
5.	Donepezil	3152	-6.727	-4.327	-2.83	-6.243	-9.194	-8.27	-2.845	-2.273
Natural compounds										
6.	Cyanidin	128861	-8.373	-4.306	-3.016	-4.291	-7.709	-4.201	-3.533	-3.743
7.	Catechin	9064	-10.137	-9.802	-3.991	-6.287	-8.191	-7.524	-4.569	-5.279
8.	Kaemopferol	5280863	-7.086	-8.96	-2.283	-3.029	-7.727	-7.378	-3.401	-4.354
9.	Genistein	5280961	-6.735	-3.998	-1.988	-2.718	-8.084	-4.748	-2.043	-3.679
10.	Epicatechin	72276	-9.256	-8.562	-3.949	-6.376	-6.826	-6.504	-	-
11.	Quarcetin 3-o-glucoside	5484066	-9.152	-7.045	-3.204	-4.326	-	-6.633	-3.616	-4.921
12.	Epicatechingallate	107905	-5.508	-5.724	-3.567	-3.476	-	-6.407	-2.73	-

S.No.	Natural compounds and commercial drugs	PubChem ID	*Neuroprotective target proteins							
			AChE		BACE		BChE		Beta amyloid	
			5EIE	5DTI	5HOX	6UVP	6QAA	6QAE	4B5E	4B41
13.	Rutin	5280805	-	-	-1.614	-3.577	-	-8.03	-3.858	-3.376
14.	Hesperetin	107905	-3.959	-5.989	-1.437	-3.067	-	-3.761	-	-
15.	Thea flavin-3—o-gallate	136825044	-3.649	-	-3.984	-3.733	-3.30	-	-4.71	-4.926
16.	Apigenin	5280443	-	-	-2.222	-2.58	-5.412	-7.359	-3.073	-
17.	Zinc	23994	-7.053	-4.761	-2.009	-3.614	-7.788	-3.193	-1.633	-4.366
18.	Herperetin	3115	-	-10.052	-1.97	-5.461	-	-8.781	-	-
19.	Kemopferol-3-orutinoside	5318767	-6.712	-8.272	-1.344	-3.588	-	-7821	-3.666	-3.004
20.	Quercetin	5280343	-6.952	-4.772	-2.288	-3.148	-7.679	-4.482	-3.068	-4.852
21.	Thea flavin-3'-gallate	136825044	-	-	-	-3.309	-	-	-4.106	-2.947
22.	Theaflavin	135403798								
23.	Gallic acid	370	-	-	-2.104	-5.808	-	-8.847	-1.474	-
24.	Caffeine	2519	-	-4.771	-	-9.204	-	-8.455	-1.908	-
25.	Kaempferide 3-glucoside	44259083	-6.734	-7.276	-3.685	-5.547	-	-6.936	-4.16	-

PubChemID : Pubchem ID of the natural compounds and commercial drugs (ligands)

***Neuroprotective target proteins**	**PDB ID of target proteins**
AChE - acetylcholinesterase	PDB ID: 5EIE, 5DTI of Acetylcholinestrase
BACE - β-secretase	PDB ID: 5HOX, 6UVP of BACE
BChE – butyrylcholinesterase	PDB ID: 6QAA 6QAE of BChE
Beta amyloid	PDB ID: 4B5E4B41 of Beta amyloid

Table IV makes it evident that five commercial drugs and fifteen carefully selected natural chemicals were utilized in molecular docking to evaluate the neuroprotective effect. Based on the analysis of docking study results, two most prominently docked compounds were identified. These include the commercial drug **rivastigmine** and natural compound **catechin**. The commercial drug rivastigmine was found to have a docking score of -7.104 and the natural compound, catechin was found to have a docking score of -10.137. These docking scores are the best compared to that of other compounds. Hence these two ligands were selected for further study.

4.1.1.6. Molecular docking of the ligands to protein acetylcholinesterase (AChE) active site

The results of the molecular docking of the ligands to protein active site are presented in Table V

Table V

Docking results of best-scored ligands with protein target

S.No	Compound name	Docking score (Kcal/mol)	No of H-bond	Amino acid associated with non- bonded interaction	Interacting residues	Bond length (A˚)
1.	Rivastigmine	-7.104	3	ASP241 SER51 ILE134 TRP131 LYS86 VAL85	GLY243 TYR211 ASN123	2.47 3.01 2.03
2.	Catechin	-10.137	3	ILE129 GLY29 THR245 LEU46 SER51 ARG28	ASP48 TYR72 GLY243	2.75 2.74 2.70

Compounds: Natural compounds and commercial drugs
Docking score: binding affinity of the compounds (Kcal/mol)
No of H-bond: hydrogen bond interactions with amino acids
Amino acid associated with Non- bonded interaction
Distance: Length of H-bond/ distance

It can be accessed from the table that the results of molecular docking studies of the commercial drug rivastigmine and natural drug catechin to acetylcholinesterase (AChE) active site. Compared to other commercial drugs such as galanthamine, tacrine, memantine and donepezil, the molecular docking of rivastigmine exhibits a high binding energy of -7.104 Kcal/mol. However, the natural compound catechin was found to have a highest binding energy of -10.137 Kcal/mol compared with the commercial drug rivastigmine and other natural compounds, cyanidin, rutin, kaemopferol, genistein, epicatechin, quarcetin 3-o-glucoside, epicatechingallate, hesperetin, theaflavin-3—o-gallate, apigenin, zinc, herperetin, kemopferol-3-orutinoside, quercetin, thea flavin-3'-gallate, theaflavin, gallic acid, caffeine and kaempferide 3-glucoside.

The commercial drug, rivastigmine was found to have four hydrogen bond interactions with amino acids GLY243, TYR211 and ASN123. Bond distances of these amino acid residues were observed to be 2.03A˚, 3.01A˚ and 2.47A˚ respectively.

The natural compound catechin was observed to have a binding distance of 2.75A˚, 2.74A˚ and 2.70A˚ with amino acids ASP48, PHE124 and GLN243 respectively. Compared to rivastigmine, catechin is found to be the most effective because of its significantly lowest binding affinity.

Figure 9 shows the molecular visualization of molecular docking poses of rivastigmine in the active site of AChE and Figure 9 (a) shows the 2D interaction of rivastigmine in the active site of AChE.

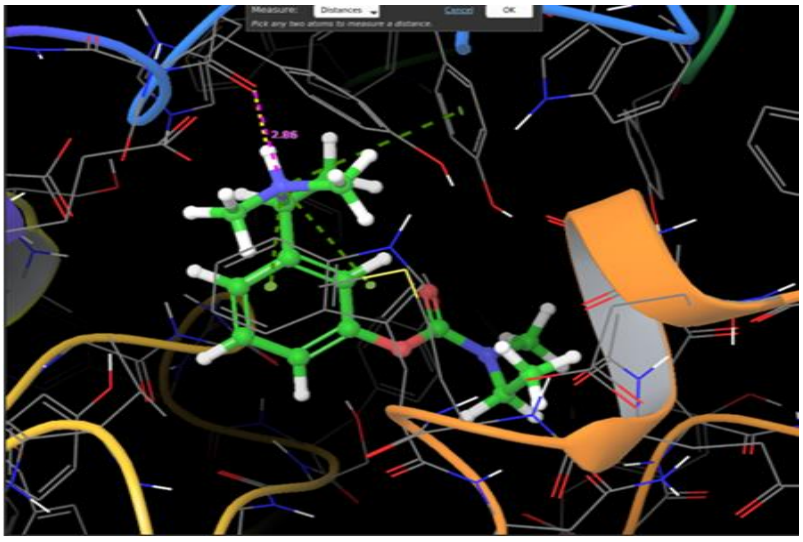

Figure 9: Docked complex structures of rivastigmine

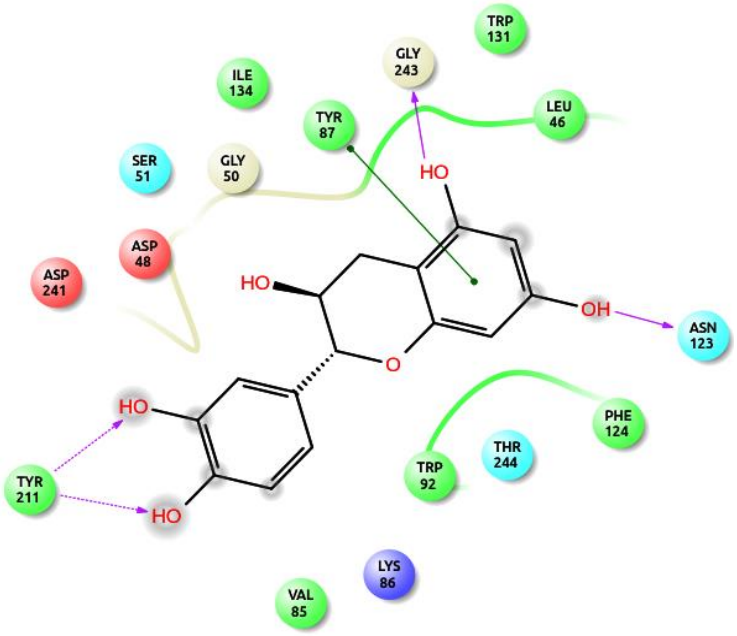

Figure 9 a): 2D interaction of AChE rivastigmine in the active site of AChE

Figure 10 shows the molecular visualization of molecular docking poses of catechin in the active site of AChE and Figure 10 (a) shows the 2D interaction of AChE catechin in the active site of AChE.

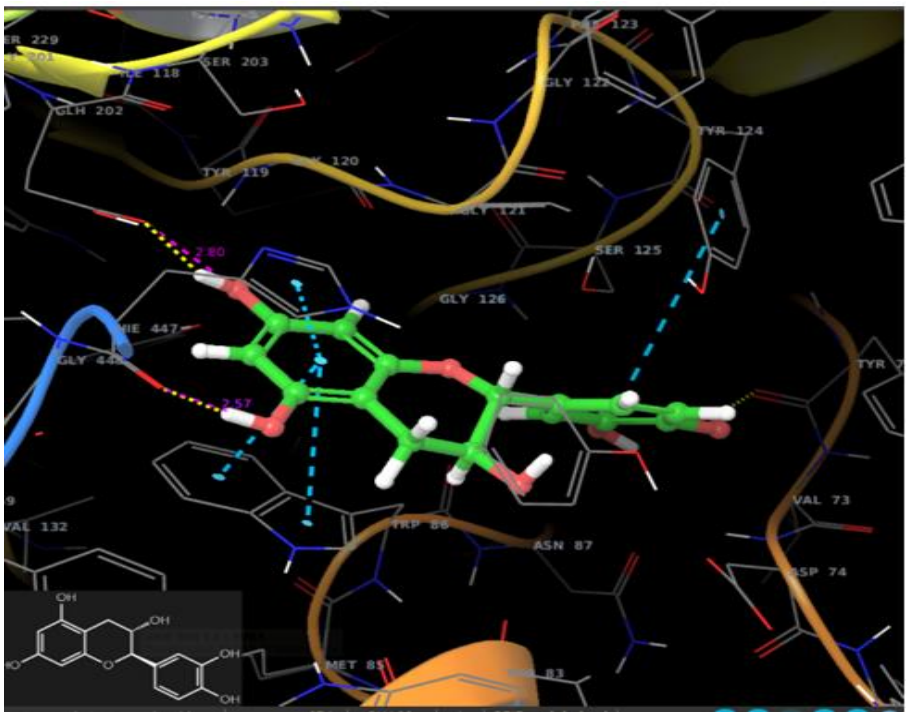

Figure 10: Docked complex structures of catechin

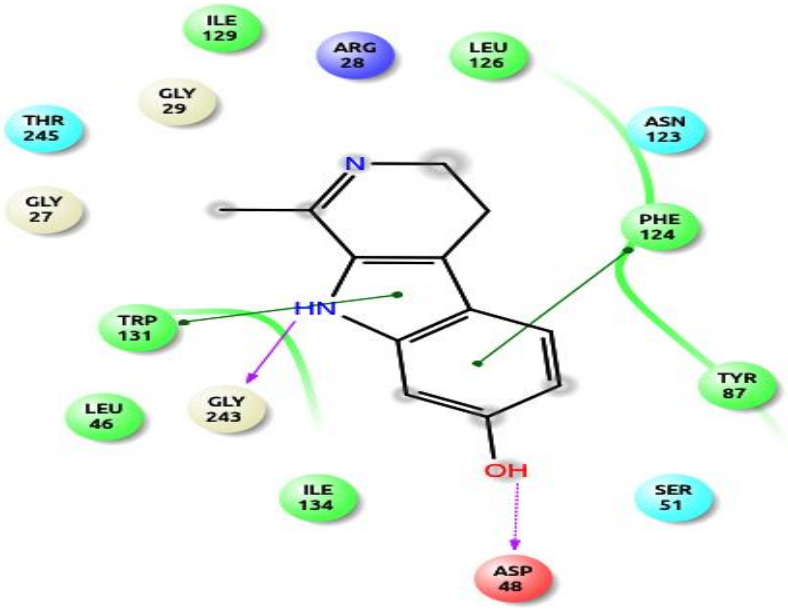

Figure 10 a): 2D interaction of AChE catechin in the active site of AChE

The results of the present study are in accordance with the study of Sheeja malar *et al.*, 2017), who mentioned that the compounds identified by LC-MS analysis were attached to the AChE, specifically with the residues ASN233, THR238, GLU313 and TRP532, hydrogen bond interaction. Vitekin's strongest docking score of 68.105 indicates that it demonstrated the highest receptor-ligand interactions among the molecules. The reported cholinesterase inhibition of the *Grewia tiliaefolia* methanol extract may be caused by these chemicals interacting with the target area. A similar report was given by Pohanka, (2014) who stated that the AChE has a better developed peripheral anionic site and a narrower aromatic gorge (The high aromatic content of the deep and narrow active-site gorge of acetylcholinesterase (AChE) is a remarkable feature of this enzyme) than butyrylcholinesterase, which explains why all of the medicines had the highest binding score when compared to their binding affinities with therapeutic target proteins. Another study by Hampel, (2012) stated that the beta-secretase mediates the breakdown of the amyloid precursor protein into small peptides which produce beta-amyloid. Therefore, beta-secretase inhibitors have the ability to halt neurological development. Comparable findings by Gu *et al.*, (2018) showed that the other docking complexes, AZD3293 with posture 8 was the most active structural position and predicted the best energy values (−5.33 kcal/mol). In addition, the intermolecular energy value (−7.42 Kcal/mol) was favourable on comparison to other conformations of docking poses.

From the above results, it could be concluded that catechin has minimum binding energy as well as inhibitory constant when compared to other compounds. Based on this, a catechin-rich plant source, namely, *Camellia sinensis* was selected for further studies.

4.2. Phase II :

Characterization of *Camellia sinensis* and identification of its bioactive compound

In this phase, different extracts of *Camellia sinensis* leaves (hexane, acetone, ethyl acetate ethanol, methanol and hydroethanolic extracts) from the field and factory were prepared and subjected to preliminary phytochemical screening for antioxidant activity, free radical scavenging activity and finally isolation of the predominant bioactive compound using column chromatography, TLC, FT-IR, GC-MS and NMR spectral techniques.

4.2.1. Qualitative screening for phytoconstituents in *Camellia sinensis*

Phytochemicals, the chemical compounds are often used to describe a large number of secondary metabolites derived from plants (Gul *et al.*, 2017). Though there are numerous phytochemicals available, only a small portion has been isolated and identified from the plants (Gomez-Garcia *et al.*, 2020).

Table VI depicts the results of the phytochemical screening of different *Camellia sinensis* leaf extracts.

Table VI

Phytochemicals in extracts of *Camellia sinensis*

S.No	Phyto-chemicals	Extracts of *Camellia sinensis* from field						Extracts of *Camellia sinensis* from factory					
		Hexane	**Acetone**	**Ethyl Acetate**	**Ethanol**	**Methanol**	**Hydro-ethanol**	**Hexane**	**Acetone**	**Ethyl Acetate**	**Ethanol**	**Methanol**	**Hydro-ethanol**
1	Alkaloids	+	++	+	+	+	++	+	+	+	+	+	+
2	Phenols	-	+	+	+	+	+	+	+	-	+	+	+
3.	Flavonoids	+	+++	++	++	++	+++	+	++	+	++	++	+++
4.	Tannin	++	+++	+++	++	+++	+++	+	+++	++	+++	+++	+++
5.	Glycosides	+	++	+	++	+	+++	+	++	+	+	+++	++
6.	Saponin	-	-	-	-	-	+	-	-	-	-	-	+
7.	Terpenoides	-	+	-	++	+	+++	-	-	+	+	++	+
8.	Steroids	+	+	+	+	+	+	+	+	+	+	+	+
9.	Phytosteroids	-	+++	+	+	+	++	-	+++	+	++	++	++

+++>++>+ Intensity of colour formation (presence of specific compounds)
- : No colour formation (absence of specific compounds)

From the table, it can be observed that all the extracts of *Camellia sinensis* from both field and factory had fairly good amounts of tannins (+++) followed by flavonoids and then glycosides. In the case of extracts of *Camellia sinensis* from fields, the hexane extract showed the presence of more of tannins, when compared to the other phyotochemicals, the acetone extract showed more of flavonoids, tannins, phytosteroids, alkaloids and glycosides, the ethyl acetate extract more of tannins and flavonoids, ethanol extract more of flavonoids, tannins, glycosides and terpenoids, methanol extract more of tannins and flavonoids and hydroethanol more of flavonoids, tannins, glycosides, terpenoids, alkaloids and phytosteroids. As regards the extracts of *Camellia sinensis* from the factory, the acetone extract had more amounts of tannins and phytosteroids followed by flavonoids and glycosides. The ethyl acetate extract had more of tannins, the ethanol extract had more of tannins followed by flavonoids and phytosteroids, the methanol extract had more of tannins and glycosides followed by flavonoids , terpenoids and phytosteroids and the hydroethanol extract had more of flavonoids and tannins followed by glycosides and phytosteroids. The amounts of phenols, saponins and steroids were very less in all the samples. The hydroethanolic extracts of *Camellia sinensis* from both the field and factory showed the presence of more phytoconstitutents than the other extracts.

Presence of phytochemicals in the leaf extracts of *Orthosiphon stamineu,* a type of tea leaf was also reported by Sivakumar and Jeganathan, (2018) who mentioned the occurence of alkaloids, anthraquinones, cardiac glycosides, flavonoids, reducing sugars, saponins, steroids, phenol, carbohydrates, tannins and anthraquinone. Phytochemical screening of the leaves of A*quilaria malaccensis* tea was also mentioned by Surjanto *et al.,* (2019) who reported the presence of tannins, alkaloids, flavonoids, saponins and triterpenoids. Xu *et al.,* (2019) also revealed the presence of preliminary phytochemicals in green tea extract. Rukshana and Pushpa, (2017) observed the presence of different phytochemical constituents in the ethanolic extract of *Pergulariadaemia* tea leaf which included alkaloids, glycosides, terpenoids, steroids, carbohydrate, tannins and flavonoids.

Thus it can be inferred from the qualitative analyses of phytochemicals that the hydro ethanolic extract of field grown *Camellia sinensis* showed the maximum presence of phytochemical constituents.

4.2.2 Quantification of phytochemical constituents of *Camellia sinensis*

Plants have been known to be used in the treatment and management of diseases due to the presence of phytochemicals (Ajayi *et al.,* 2017). Phenolic compounds are important plant constituents with redox properties responsible for antioxidant activity (Aryal *et al.,* 2019). Flavonoids are secondary metabolites that have an antioxidant effect, the strength of which is determined by the amount and position of free OH groups (Panche *et al.*, 2016). Hence in the present study, the content of phenols and flavonoids in the hexane, acetone, ethyl acetate ethanol, methanol and hydroethanolic extracts of *Camellia sinensis* were estimated.

4.2.2.1. Total phenol content

Table VII and Figure 11 depict the total phenol content in the hexane, acetone, ethyl acetate ethanol, methanol and hydroethanol leaf extracts of *Camellia sinensis.*

Table VII

Total phenolic content of *Camellia sinensis*

S.No.	Extracts	Total phenol content (mg/ml) *
1.	Hexane	1.714±0.06
2.	Acetone	2.021±0.02
3.	Ethyl acetate	8.687±0.21
4.	Ethanol	10.59±1.21
5.	Methanol	13.21±1.22
6.	Hydroethanolic	15.90±1.40

Values are mean ±SD of triplicates * significant at p <0.05

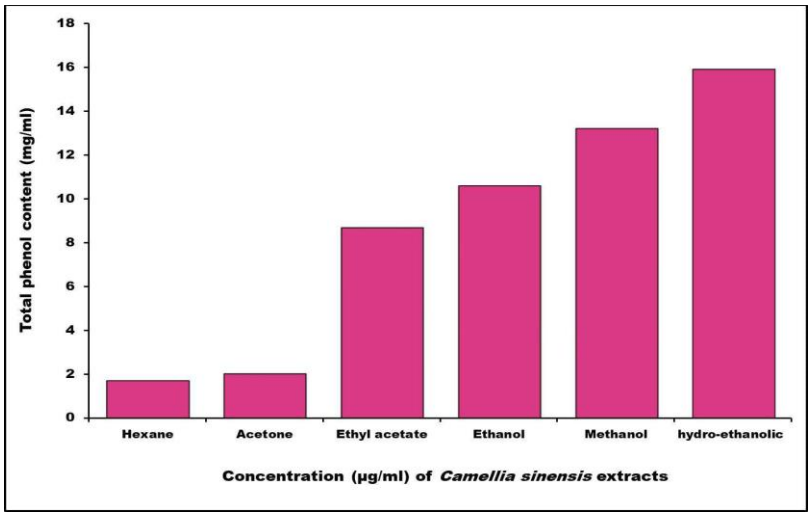

Figure 11: Total phenol content of *Camellia sinensis*

From the table and figure it can be stated that phenol as present in all extracts (hexane, acetone, ethyl acetate, ethanol, methanol and hydroethaolic) of *Camellia sinensis* with significantly ($p<0.05$) highest content in the hydroethaolic extract (15.90±1.40 mg/ml) followed by methanol extract (13.21±1.22 mg/ml).

The presence of phenols in green tea was also reported by Kaur *et al.*, (2015), Kodama *et al.*, (2010); Anesini *et al.*,(2008); Shrestha *et al.*, (2010), Izzreen and Fadzelly, (2013).

It can thus be inferred from the study that the total phenol content was highest in the hydroethanolic extract of *Camellia sinensis* when compared to than the other extracts.

4.2.2.2. Total flavonoid content

Table VIII and Figure 12 depict the total flavonoid content in the hexane, acetone, ethyl acetate, ethanol, methanol and hydroethanolic leaf extracts of *Camellia sinensis.*

Table VIII

Total flavonoid content of *Camellia sinensis*

S.No.	Extracts	Total flavonoid content (mg/ml)
1.	Hexane	42.18±1.37*
2.	Acetone	41.62±1.32*
3.	Ethyl acetate	84.16±2.87*
4.	Ethanol	81.84±2.81*
5.	Methanol	64.72±1.97*
6.	Hydroethanolic	90.40±2.95*

Values are mean ±SD of triplicates * significant at $p<0.05$

From the table and figure, it can be observed that the hydroethanolic extract of *Camellia sinensis* had the highest quantity (90.40±2.95 mg/ml) of flavanoids which was significant ($P<0.05$) followed by ethyl acetate extract (84.16±2.87 mg/ml) when compared to the other extracts (hexane, acetone, ethanol and methanol).

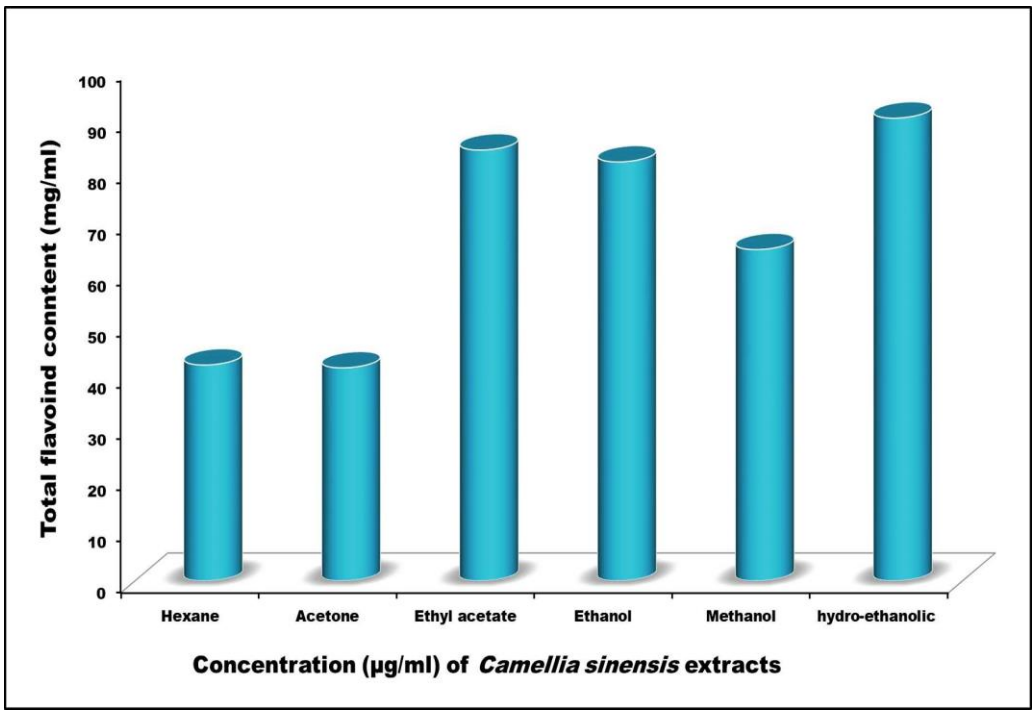

Figure 12: Total flavonoid content of *Camellia sinensis*

Presence of flavonoids in different types of tea extracts was also reported by Wen *et al.,* (2023), Bakar *et al.,* (2014) and Ling *et al.,* (2010). The amount of total flavonoids in hexane and acetone extracts of *Camellia sinensis* as reported in the present study (42.18±1.37 and 41.62±1.32 respectively) agrees with the results of Bansode, (2015) who also reported 48.81 mg/mg of flavanoids in Parichaya golden black tea.

It can thus be inferred from the results of flavonoid content in different extracts of *Camellia sinensis* that the highest amount of flavonoids was present in the hydroethanolic extract.

4.2.3. Antioxidant Radical Scavenging activity

4.2.3.1. Diphenyl-Picryl Hydrazine (DPPH) radical scavenging activity in *Camellia sinensis*

The DPPH assay is a simple, acceptable and frequently utilized method for determining the radical scavenging efficacy of substances or plant extracts (Dudonne *et al.*, 2009). The violet colour of the DPPH radicals decrease to yellow-coloured diphenylpicrylhydrazine radicals when the stable DPPH radicals accept electrons from the

antioxidant substance. The substances that possess a capacity to carry out this reaction are known as radical scavengers or antioxidants (Sasikumar and Kalaisezhiyen, 2014).

Figure 13 (a) shows the IC50 values of Diphenyl-Picryl Hydrazine (DPPH) radical scavenging activity in *Camellia sinensis.*

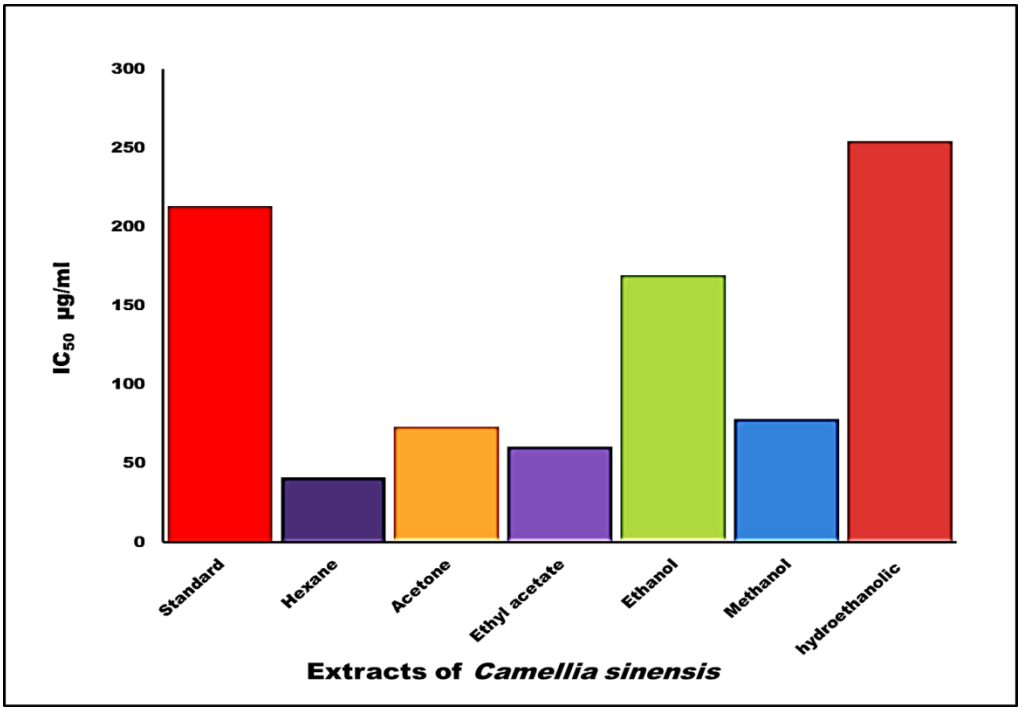

Figure 13 (a): IC 50 values of DPPH radical scavenging activity of *Camellia sinensis*

IC 50 values of DPPH radical scavenging activity of hexane, acetone, ethyl acetate ethanol, methanol and hydroethanolic extracts from *Camellia sinensis* as depicted in the figure show that the maximum IC50 value was exhibited by the hydroethanolic extract (254.10 µg/ml) followed by the ethanolic extract (169.02 µg/ml).

Figure 13 (b) shows the Diphenyl-Picryl Hydrazine (DPPH) radical scavenging activity in *Camellia sinensis.* The inhibition percentage (IP) and inhibition concentration (IC50) values are considered to be a good measure of the antioxidant efficiency of pure compounds and extracts

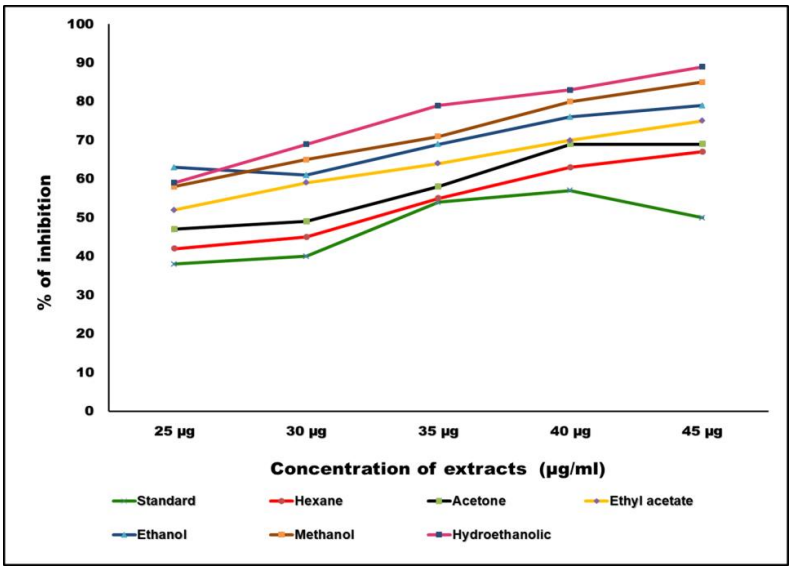

Figure 13 (b). DPPH radical scavenging activity of *Camellia sinensis*

The figure shows that the DPPH assay was performed using varying concentrations (25, 30, 35, 40 and 45 µg/ml) of hexane, acetone, ethyl acetate, ethanol, methanol and hydroethanolic extracts of *Camellia sinensis* with ascorbic acid as the standard. The results revealed that all the tested samples and standard were able to scavenge DPPH radicals in a dose dependent manner. The samples were able to scavenge the DPPH radicals even in the lowest concentration and the scavenging ability was found to be increased with increase in concentration which clearly depicts the dose dependent activity of the samples. Among the tested samples, the hydroethanolic extract was found to possess the highest DPPH scavenging activity (89%), followed by methanol (85%) and ethanol (79%) extracts. The results of the DPPH radical scavenging ability clearly indicates that all the samples tested shared electrons with the DPPH radicals by exhibiting scavenging ability.

The maximum inhibition of DPPH activity of 89 % by the hydroethanolic extract of *Camellia sinensis* as reported in the present study is on par with the study of Mety and Mathad (2011), who stated that the methanolic extracts of bark and fruit pulp of all the species of *Terminalia* (Terminalia is a genus of big trees of the blooming trees) showed maximum inhibition percentage values ranging from 94 -95.

It can thus be inferred from the above study that the maximum percentage inhibition of DPPH scavenging activities was revealed by the hydroethanolic extract of *Camellia sinensis* with increase in a dose-dependent manner when compared to other extracts.

4.2.3.2 Ferric Reducing Antioxidant Power (FRAP) radical scavenging activity in *Camellia sinensis*

FRAP assesses the reduction of ferric ion (Fe3+)-ligand complexes by antioxidants in an acidic solution to the strongly blue-coloured ferrous (Fe2+) complex (Zhong and Shahidi, 2015).

The results of the FRAP assay with *Camellia sinensis* extracts of hexane, acetone, ethyl acetate, ethanol, methanol and hydroethanolic are recorded in Figure 14.

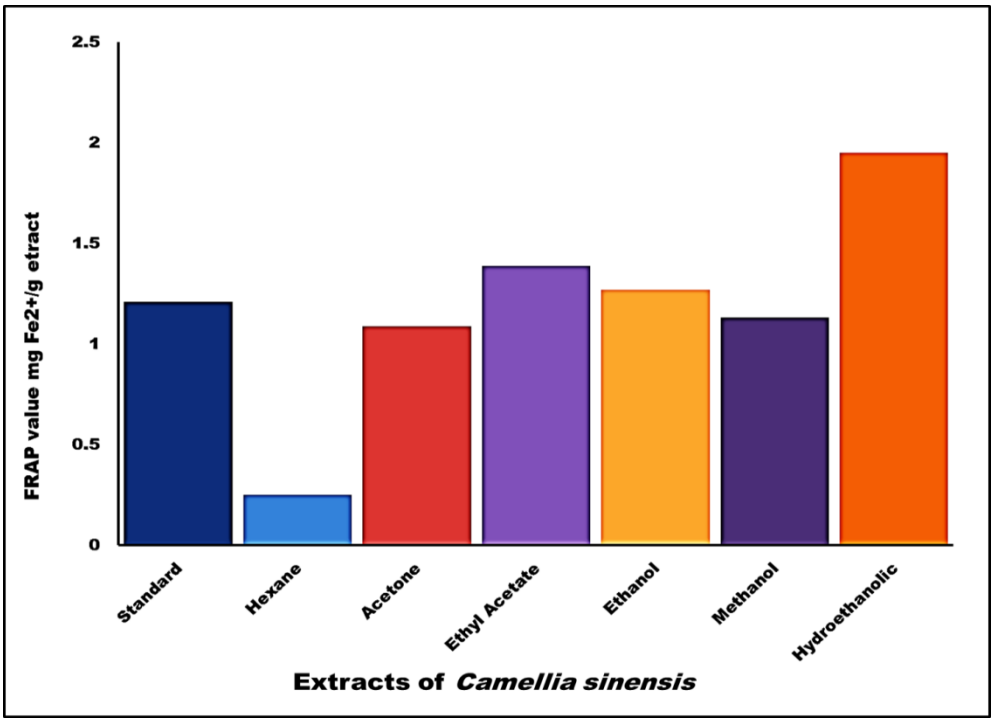

Figure 14: FRAP radical scavenging activity of *Camellia sinensis*

From the figure, it can be deduced that the hydroethanolic extract of *Camellia sinensis* revealed the maximum antioxidant potential (1.95 mmol Fe II/g) followed by the ethyl acetate extract (1.39 mmol Fe II/g).

The above results are on par with the work of Tang *et al.*, (2019) who reported that in the various solvent extracts of 30 common Chinese tea varieties, the FRAP mean value was found to be 1.14 mmol Fe II/g for a species of black tea, 1.12 mmol Fe II/g for varied types of dark tea, 1.09 mmol Fe II/g for different types of white tea and 2.01 mmol Fe II/g for oolong tea varieties. A report by Lilachjini and Haniffa, (2023) and Imran *et al.*, (2021) also

observed that the FRAP values for nine different combinations of prepared herbal tea, green tea and black tea were found to be in the range of 0.65 to 0.812 mmol Fe II/g.

It can thus be concluded from the results of FRAP radical scavenging activity that the hydroethanolic extract of *Camellia sinensis* had the highest radical scavenging activity.

4.2.3.3 Total Antioxidant Capacity (TAC) in *Camellia sinensis*

Total antioxidant capacity is a common analyte used for evaluating the antioxidant status of biological samples and the antioxidant response to the free radicals released in a particular disease (Rubio *et al.*, 2016).

Figure 15 presents the total antioxidant capacity of different extracts of *Camellia sinensis.*

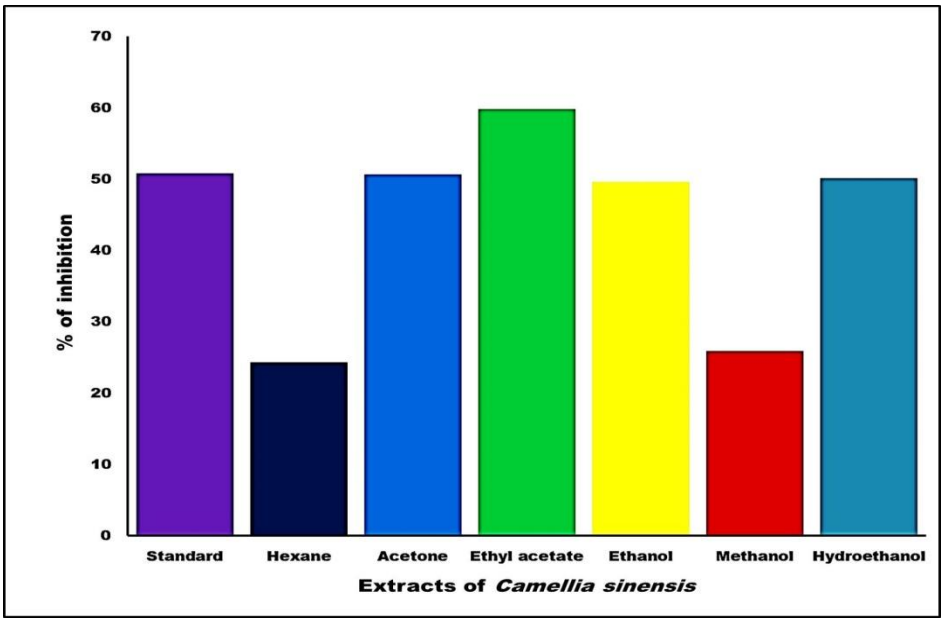

Figure 15: Total antioxidant capacity of *Camellia sinensis*

It is understood from the figure that the IC 50 value of the ethyl acetate extract of *Camellia sinensis* was found to be the highest (60%) followed by acetone and hydroethaolic extracts when compared to the other extracts of *Camellia sinensis*.

The finding of the present study that the maximum inhibition by C*amellia sinensis* was 60% is quite similair to the study conducted by Phull *et al.*, (2021) who also worked with a medicinal plant *Forsythia koreanaI* (Korean goldenbell tree) and reported a total

antioxidant capacity range of 11.2 to 92.3 %. A study by Kiran (2018) on green tea samples also reported a total antioxidant capacity of 22.86.

It can thus be stated that the total antioxidant capacity was maximum in the hydroethanolic extract of *Camellia sinensis* as compared to the other extracts.

4.2.4. Enzymatic antioxidants in *Camellia sinensis*

Enzymatic antioxidants act by decreasing and removing free radicals. Plants have constructed an extensive defense mechanism comprising of number of enzymatic antioxidants such as catalase, glutathione, superoxide dismutase, ascorbate peroxidase and guaiacol peroxidase (Nimse and Pal, 2015; Bacha *et al.* 2017).

The dried powder from *Camellia sinensis* leaves were used to estimate the enzymatic antioxidants and non-enzymatic antioxidants.

Table IX registers the enzymic antioxidant levels of *Camellia sinensis*

Table IX

Enzymic antioxidants of *Camellia sinensis*

Enzymic antioxidants	Activity
[#]Catalase	122.57 ± 26.72 U/g*
[$]Super oxide dismutase	69.43 ± 18.05 [NS]
[@]Polyphenol oxidase	1.75 ± 0.20 mmol/min*
[^]Glutathione peroxidase	5.73 ± 0.50 µmol/min*
[+]Glutatione -S -transferase	2.52 ± 0.47 µmol/min [NS]

*-Significant at 5% level
NS- Not significant
1 Unit = Amount of enzyme required to decrease the absorbance at 240nm by 0.05 units/minute
$1 Unit = Amount of enzyme that causes 50% reduction in NBT oxidation
@ 1 Unit = Millimoles of NADPH oxidized/minutes
^ 1 Unit = µ mole of GSH consumed/minute
+ 1 Unit = µ mole of CDNB conjugated/minute

The table above indicates that the leaves of *Camellia sinensis* were found to exhibit significant (P>0.05) activity of catalase (122.57±26.72 U/g). As regards polyphenol oxidase, the leaves of *Camellia sinensis* were found to have a significant value of 1.75±0.20 mmol/min. In the case of Glutathione S-transferase, the activity was found to be 2.52±0.47 µmol/min in the leaves of *Camellia sinensis*. The superoxide dismutase activity of *Camellia*

sinensis leaves was found to 69.43±18.05 % followed by Glutathione peroxidase (5.73±0.50 µmol/min).

A similar value of catalase was evident in the results of Das *et al*., (2017) who portrayed clearly that the catalase activity of enzymatic antioxidants in the leaves of oats was found to be 127.33 U/g. In the case of SOD the present study showed a value of 69.43 % which was in accordance with the value (72.45 %) reported by Gangwar *et al*., (2014) in the extract of *Mallotus philippenensis* (a fruit tree). Basar *et al*., (2022) evaluated polyphenol oxidase activity in the leaf, flower, stem, bark and root of *Justicia adhatoda* and reported a value of 1.04 ± 0.87 U/mg of fresh weight. The results of the present study showing a value of 2.52 µmol/min for glutathione -S- transferase also agrees with the studies of Rajan and Pushpa, (2015), who reported the activity of glutathione -S- transferase to be 2.908 µmol/min in the seed extract of Java fruit .

It can thus be inferred from the study that *Camellia sinensis* leaves had a good amount of enzymic antioxidants.

4.2.5. Non-enzymatic antioxidants in *Camellia sinensis*

Non-enzymatic antioxidants work by interfering with the chain reactions of free radicals. Non-enzymatic antioxidants such as ascorbate, carotenoids, flavonoids and other phenolics are used to counteract the negative effects of oxidative damage (Zhong and Shahidi, 2015).

Table X depicts the non-enzymatic antioxidants present in *Camellia sinensis.*

Table X

Non-enzymatic antioxidants of *Camellia sinensis*

Non-enzymatic antioxidant	Activity
Ascorbic acid	1.72±0.32 (mg/g)^{NS}
Tocopherol	3.16±1.22 (µg/g)*
Flavonoids	25.23±3.36 (mg/g)*
Polyphenols	22.27±2.66 (mg/g)*
Reduced glutathione	165.20±11.81 (nmoles)*

Values are mean ± SD of five samples
*- Significant at P >0. 05% level NS- Not significant

From the table it is understood that the leaves of *Camellia sinensis* exhibited significant amounts of all the non-enzymatic antioxidants - tocopherol, flavonoids, polyphenols and reduced glutathione. The ascorbic acid content of the leaves of *Camellia sinensis* was found to be 1.72±0.32 mg/g, the α-tocopherol content 3.16±1.22 µg/g, the flavonoids content 21.23±3.36 mg/g and reduced glutathione level 165.20±11.81 nmoles in the leaves of *Camellia sinensis.*

The present finding that the ascorbic acid level in *Camellia sinensis* was 1.72±0.32 mg/g is similar to the results of Jadhao and Poonam, (2016) who reported a value of 1.73 mg/g in the leaves of *Abrus precatorious* (Rosary pea), 1.37 mg/g in *Boerhavia diffusa* (punarnava herb) and 1.73 mg/g in *Begonia crenata* (succulent herb). The flavonoid content of 25.23±3.36 mg/g as obtained in the present study was similar to the value reported by Obouayebab *et al.* (2015) who stated that the flavonoid content in a type of *Hibiscus sabdariffa* species was 20.70 ±1.50 mg/g.

Thus, from the above results it can be deduced that the leaves of *Camellia sinensis* had a fairly good amount of non-enzymic antioxidants.

It was thus justified that the combination of water and ethanol solvent gives better extraction of polyphenols than water alone. The present study also showed that the hydroethanolic extract of *Camellia sinensis* leaves is a good radical scavenger and an effective antioxidant agent, as a result of which this extract was selected for the studies that followed.

4.2.6. Active constituent in *Camellia sinensis*

The hydroethanolic extract of *Camellia sinensis* leaves selected was run by column chromatography and the fractions collected. These fractions were than subjected to TLC to identify the active component. The selected fraction was further analyzed by HPTLC, UV, FTIR, GC-MS, NMR and LC-MS

4.2.6.1. Results of column chromatography analysis of *Camellia sinensis* extract

The hydroethanolic extract of *Camellia sinensis* was fractionated by column chromatography using hexane: ethyl acetate solvent system in the ratio 80:20 to enable qualitative and quantitative separation, identification and purification of compounds and the fractions collected were subjected to TLC.

The results of these are shown in Table XI and Plate 2.

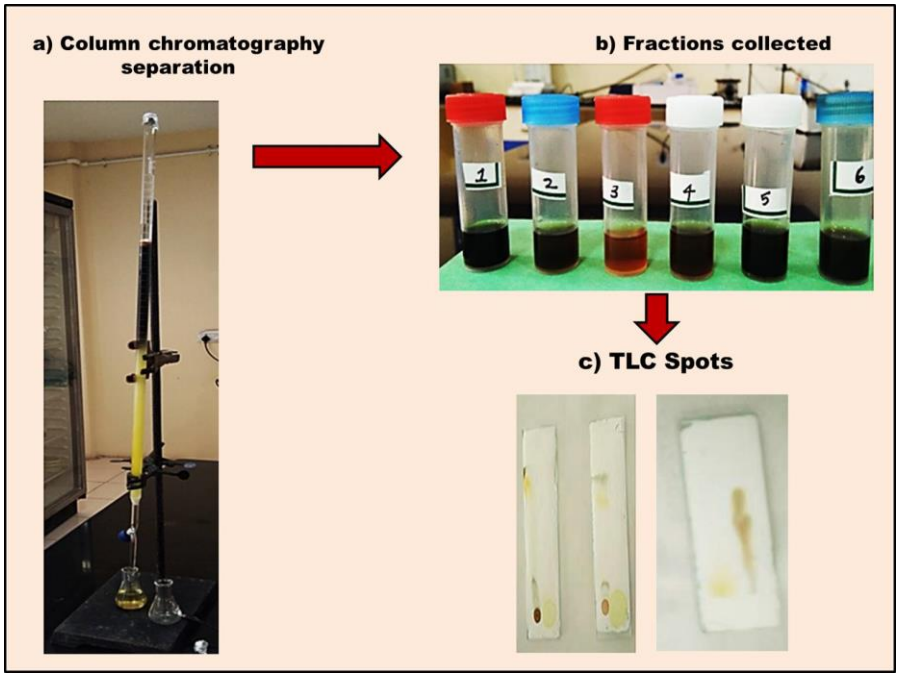

a) Column Chromatography b) Fractions collected c) TLC spots

Plate 2. Column Chromatographic patterns of hydroethanolic extract of *Camellia sinensis*

Table XI

Rf values after TLC of *Camellia sinensis* column chromatographic fractions

Samples	Spots	Fractions	Rf values
Catechin	**S**	**-**	**0.67**
Hydroethanolic extract of *Camellia sinensis*	1	1-45	0.76
	2	46-68	0.79
	3	69-80	**0.67**
	4	81-89	0.73
	5	90-119	0.65
	6	120-135	0.29

It was observed from Table XI and Plate 2 that 135 fractions were obtained after column chromatography of the sample. These fractions were pooled to get six fractions by combining fractions 1-45, 46-68, 69-80, 81-89, 90-119 and 120-135 and subjected to Thin Layer Chromatography (TLC) with catechin as the standard.

From the Rf values of the spots obtained, it can be noticed from Table XI that the Rf value of fraction 3 (0.67) corresponded to the Rf value of the standard catechin (0.67) proving that the active constituent present in *Camellia sinensis* leaves is catechin.

The presence of catechin in the column chromatographic fractions of *Camellia sinensis* as observed in this study agrees with the results of Royani *et al.,* (2023) who mentioned that the major chromatographic fractions of fermented tea extract contains catechin gallate and epicatechin gallate. The above study is also supported by Sah *et al*., (2014) who stated that the TLC fraction of the petroleum ether and chloroform extracts of *Durio zibenthinus* (Durian fruit) showed similar spots ensuring the separation of catechin. A study by Ligor *et al.,* (2008) also mentioned that in TLC of green tea extract particular flavonoid constituents such as myrectin, rutin, catechin, querectin and kaemoferol were seen with Rf value of catechin.

Hence, it is confirmed by column chromatography and thin layer chromatography that the active constituent catechin was present in the 3rd chromatographic fraction of the hydroethanolic extract of *Camellia sinensis.*

Since the active component was present in the 3rd column chromatographic fraction of the hydroethanolic extract of *Camellia sinensis,* this fraction was further characterized by subjecting it to HPTLC, UV, FT-IR, GC-MS, NMR and LC-MS.

4.2.6.2. Results of HPTLC analyses of selected chromatographic fraction of *Camellia sinensis* extract

High Performance Thin Layer Chromatography is capable of analyzing multiple samples simultaneously, even those with different components (Arage *et al.,* 2023) and it proves to be a linear, precise and accurate method.

Table XII records the HPTLC peaks of the selected chromatographic fraction of the hydroethanolic extract of *Camellia sinensis* and Figure 16 depicts the baseline display and peak densitogram display of catechin. Figure 17 represents the superimposed HPTLC fingerprints of catechin in the selected chromatographic fraction of the hydroethanolic extract of *Camillia sinesis* leaves**.**

Table XII

HPTLC peaks of selected chromatographic fraction of hydroethanolic extract of *Camellia sinensis*

Track	Peaks	Rf	Height	Area	Assigned substance
E	1	0.05	140.4	3753.7	**unknown ***
	2	0.18	332.7	20391.7	**unknown ***
	3	0.29	175.3	6122.1	**unknown ***
	4	0.37	174.1	6722.9	**unknown ***
	5	0.43	68.9	1262.1	**Catechin**
	6	0.47	55.3	810.1	**unknown ***
	7	0.50	58.5	1341.9	**unknown ***
	8	0.55	70.0	1674.3	**unknown ***
	9	0.63	78.4	4769.7	**Rutin**
	10	0.75	48.2	1747.2	**unknown ***
	11	1.02	73.8	2951.0	**unknown ***
	12	1.09	217.2	5458.8	**unknown ***
	1	0.47	417.9	19551.7	**Catechin**
		1.13	**87.5**	**4794.0**	**Rivastigmin**

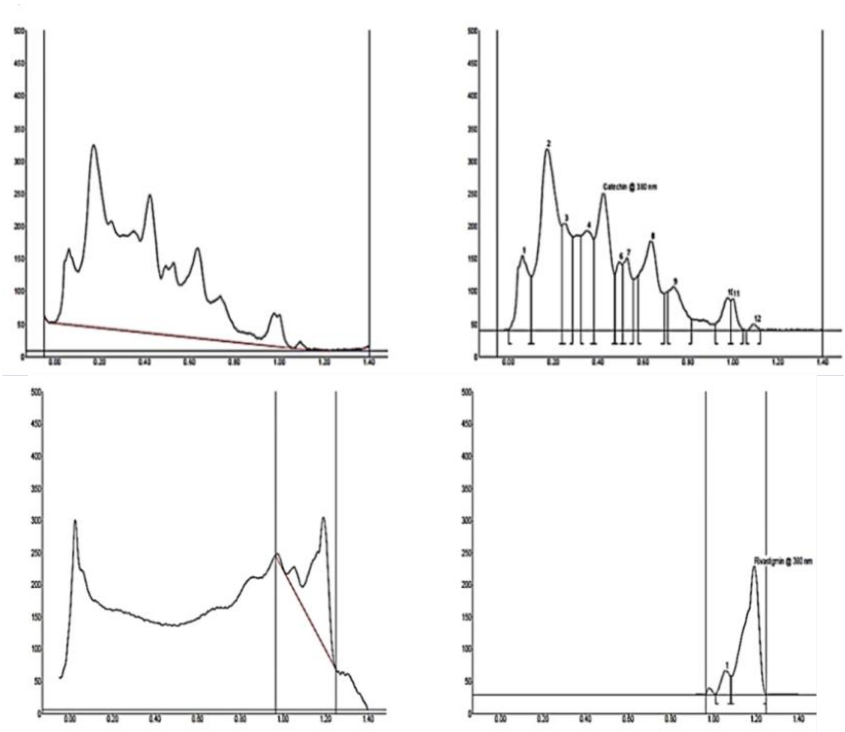

Figure 16: Track 1 Baseline display and peak densitogram display of catechin

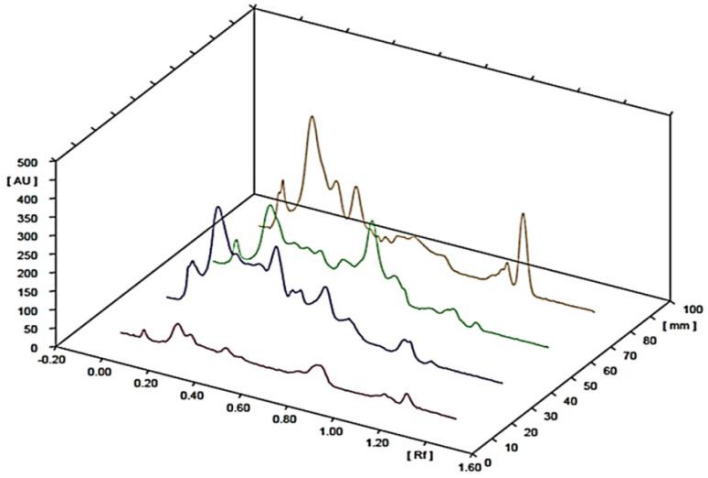

Figure 17: 3D display of HPTLC superimposed HPTLC fingerprints of catechin

From Table XII, it can be clearly stated that the chromatogram and peak densitogram display of the sample obtained through HPTLC showed that out of the 12 peaks obtained from the hydroethanolic extract of *Camillia sinesis* leaves, the 5^{th} peak with an Rf value of 0.43 was found to correspond to that of catechin which had a Rf value of 0.47 .

Studies by Nile and Park, (2014); Thammarat *et al.,* (2021) and Mulaudzi, *et al.,* (2022) reports similar kinds of results with HPTLC fingerprints of betel leaf extract. Another finding of the present study showing catechin to be the main active component is on par with the work of Morlock *et al.,* (2021) who also reported the presence of catechin as well as gallocatechin, catechin-3-gallate, epicatechin, epicatechin-3-gallate, epigallocatechin and epigallocatechin-3-gallate in the 10^{th} and 11^{th} peaks of the histogram obtained through HPTLC study of methanolic extracts of 20 *Camillia sinesis* leaves.

The above findings confirm the presence of catechin in the selected chromatographic fraction *Camillia sinesis.*

4.2.6.3. Results of ultraviolet–visible spectroscopy analysis of selected chromatographic fraction of *Camellia sinensis*

Qualitative and quantitative analysis of the selected chromatographic fraction of *Camellia sinensis* were carried out by studying the peaks obtained from 200-1200 nm by UV-Vis spectroscopy.

Figures 18 depicts the UV spectrum of the selected chromatographic fraction of the hydroethanolic extract of *Camellia sinensis.*

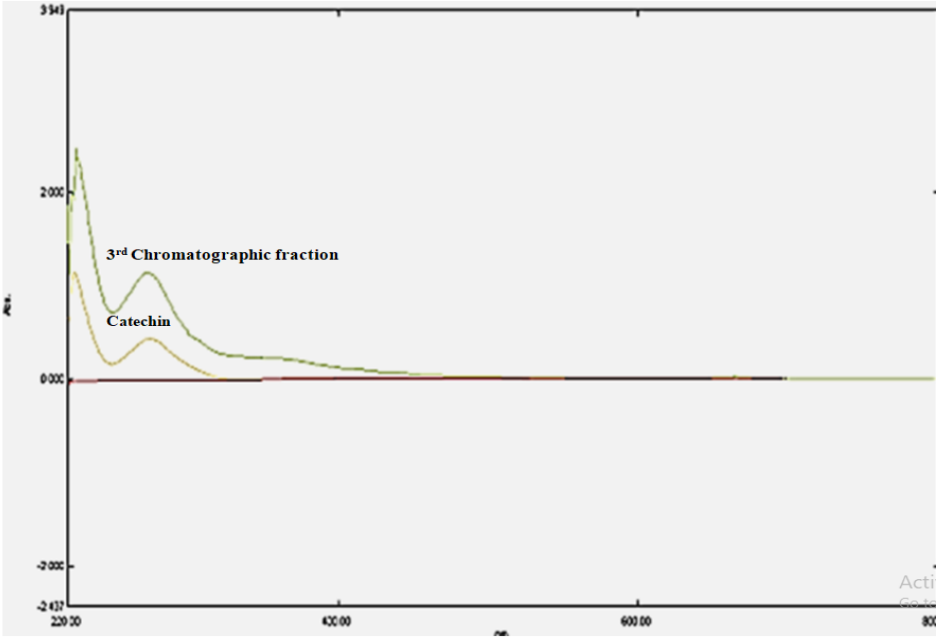

Figure 18: UV spectrum of the selected chromatographic fraction of *Camellia sinensis*

It can be seen from the figure that the absorption spectrum of the selected chromatographic fraction and standard catechin revealed a strong absorbance at 280 nm. This indicates the presence of a bioactive compound in the selected chromatographic fraction.

The present results are in accordance with the reports of Ibrahim *et al.,* (2017) who stated that catechin in green tea and herbal tea formulations gave an UV spectrum with a maximum peak at 274 nm corresponding to catechin using spectrophotometric method. Another study by Arifah *et al*., (2022) inferred that UV visible spectroscopy could be used to differentiate Indonesian tea, black tea and green tea all of which gave maximum absorption peaks at 275 nm which corresponded to catechin. Yet another study by Atomssa and Gholap, (2015) mentioned that the UV visible spectrum of Ethiopian green tea and Sri Lankan green tea showed the Ethiopian green tea to have a higher catechin content than Sri Lankan green tea.

Hence from the above findings it is clear that a strong absorption peak at 280 nm was seen in the UV-visible spectrum of the selected chromatographic fraction of the hydroethanolic extract of *Camillia sinesis*

4.2.6.4. Catechin content in *Camillia sinesis*

Catechin, the main bioactive compound present in the selected chromatographic fraction of the hydroethanolic extract of *Camillia sinensis* was quantified and the results presented in Figure 19 a.

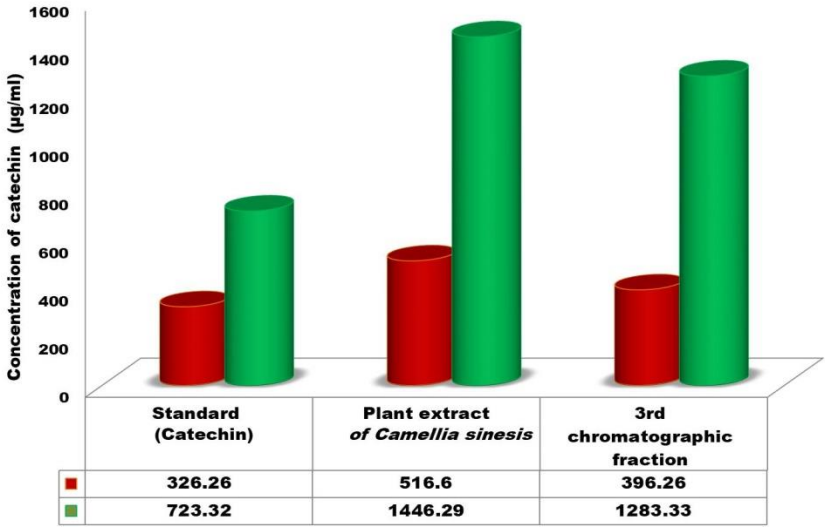

Figure 19 a). Content of catechin in 3rd chromatographic fraction of *Camillia sinensis*

It is clear from the figure that the highest catechin content was recorded by the *Camillia sinensis* extract with a value of 1446.29 µg/ml, while the 3rd chromatographic fraction showed a catechin content of 1283.33 µg/ml.

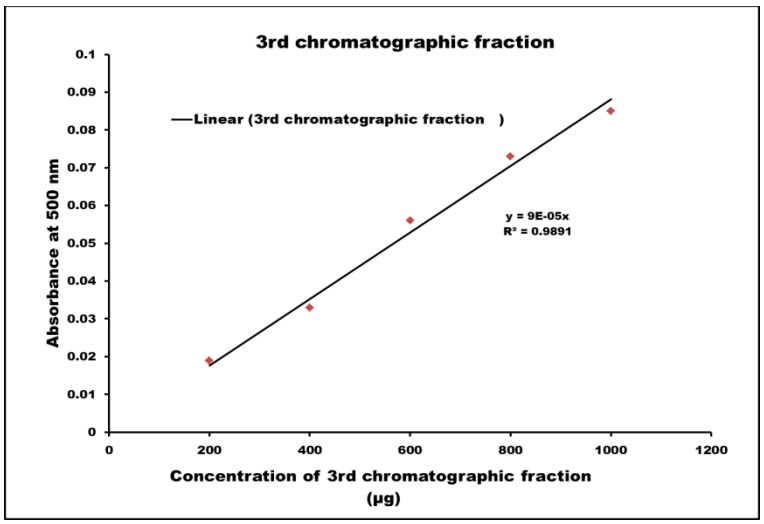

Figure 19 b. Calibration curve of the absorbance against the concentrations of catechin of *Camillia sinensis*

Figure 19 b illustrates the calibration of the absorbance against the concentration of catechin.

It can thus be seen from the figure that, the R2 value was 0.989 indicating that there is a strong correlation between absorbance and vanillin concentration. Hence the presence of catchin in the 3rd fraction was confirmed.

An R2 value of 0.989 as observed in the present study agrees with the results of a study by Maslov *et al.,* (2021) and Kalidass *et al.,* (2021), who also stated that the calibration curve of epigalllocatechin gallate showed a value of r2= 0.9975 and that of catechin showed a value of r2=0.9964. Another study by Tiwari *et al.* (2014), mentioned that certain herbal flowers like globe amarnath, hibiscus, rose, butterfly pea (white and blue) and garden mum contains catechin in their fresh and dried methanolic extracts.

This result proves that catechin is present in the 3rd column chromatographic fraction of the hydroethanolic extract of *Camellia sinensis*.

4.2.6.5. Results of FT-IR spectroscopy of the selected chromatographic fraction of *Camellia sinensis* extract

FTIR spectroscopy has been regarded as a reliable and sensitive approach for identifying functional groups in samples and they are determined using the IR region 400-4000cm-1(Hemmalakshmi *et al.,* 2017).

Figure 20 displays the Fourier-Transform InfraRed spectrum of the selected chromatographic fraction of the hydroethanolic extract of *Camellia sinensis*.

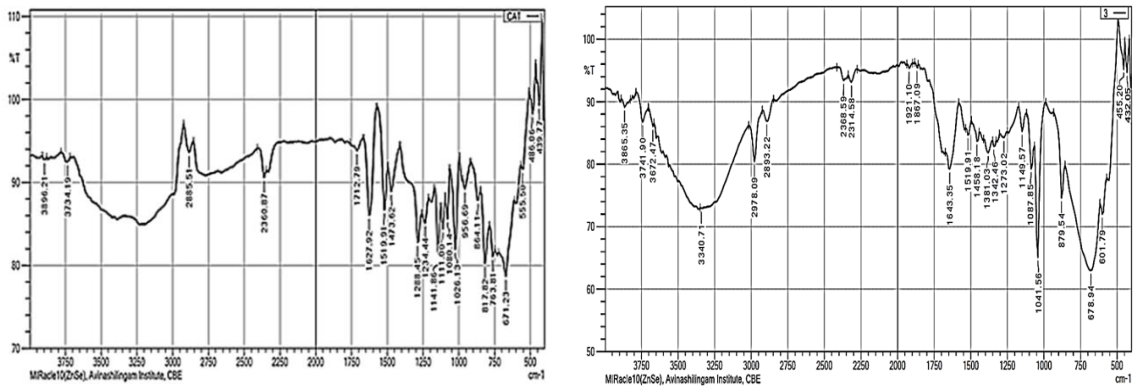

Figure 20: Fourier-Transform Infrared spectrum of the selected chromatographic fraction of *Camellia sinensis*.

It is clear from the figure that the absorption bands at 3390-3228 cm^{-1} represent O-H stretching alcohol and carboxylic acid. The absorption peak is located at around 2773 cm^{-1} representing –O-H stretching carboxylic acid. The stretching vibration present at 1643 and 1701 cm^{-1} are associated with C=O stretch vibration of amides and aldehydes respectively. The strong absorption peaks at 1361 and 1226 cm^{-1}which are assigned to CH $(CH_3)_2$ stretching alkanes and alkyls and =C-O- symmetric and asymmetric stretch ethers. Small bands were presents at 1504, 929 and 821cm^{-1} representing N-H stretching amides, =C-H- stretching alkanes and C-H stretching vibration of aromatic compounds respectively.

In accordance with the present results that *Camellia sinensis* contain catechin the findings of Wirwis and Sadowski, (2023) also reported that green tea extraction made by water validates the presence of gallic acid, catechin, alcohols, phenols and alkenes. The FTIR spectrum as obtained in this study is similar to the FTIR spectrum of six green tea samples which revealed the presence of O–H stretch, H –bonded (phenols, alcohols, C=O stretch (flavonoids, polyphenols, catechins), C–H stretch (alkanes), O–H stretch (carboxylic acid), C–H stretch (alkanes) as reported by the researcher (Senthil *et al*., 2017). A similar report by Arifah *et al*., (2022) mentioned that in the FTIR spectrum of black and green brewed tea, the C=O stretch indicates carbonyl group, C-H stretching indicates alkanes and O-H stretching indicates phenols.

The functional groups observed in the FTIR spectrum of the chromatographic fraction of the hydroethanolic extract of *Camellia sinensis* corresponds to the FT-IR spectrum of catechin confirming the presence of catechin in *Camellia sinensis*.

4.2.6.6. Results of GC-MS analysis of chromatographic fraction of *Camellia sinensis* extract

GC-MS is one of the best, rapid and accurate techniques for detecting many different substances including alcohols, alkaloids, nitro compounds, long chain hydrocarbons, organic acids, steroids, esters and amino acids (Konappa *et al.,* 2020).

The GC-MS profile of the compounds identified with retention time for the different peaks obtained in the chromatogram of the chromatographic fraction of *Camellia sinensis* extract were integrated and compared with the database of the spectrum of known components stored in the GC-MS NISP library.

Table XIII and Figure 21 show the GC-MS profile of the selected chromatographic fraction hydroethanolic extract of *Camellia sinensis*

Table XIII

GC-MS profile of the selected chromatographic fraction of *Camellia sinensis* extract

S.No.	RT	Scan	Height	Area	Area %	Norm %
1	8.346	1109	1,773,939,072	174,531,056.0	9.765	52.33
2	8.381	1116	1,805,577,472	86,312,592.0	4.829	25.88
3	8.496	1139	1,835,200,256	333,496,576.0	18.659	100.00
4	8.661	1172	1,682,891,008	90,004,296.0	5.036	26.99
5	8.826	1205	1,510,344,192	218,059,856.0	12.200	65.39
6	8.916	1223	1,361,153,408	85,306,536.0	4.773	25.58
7	8.936	1227	1,324,725,120	180,506,800.0	10.099	54.13
8	9.141	1268	1,155,558,912	133,643,344.0	7.477	40.07
9	9.271	1294	1,033,878,016	37,344,188.0	2.089	11.20
10	9.301	1300	925,263,808	71,203,264.0	3.984	21.35
11	9.436	1327	786,849,024	72,549,424.0	4.059	21.75
12	9.536	1347	640,717,312	53,715,208.0	3.005	16.11
13	9.706	1381	519,479,776	69,457,376.0	3.886	20.83
14	9.771	1394	462,718,752	42,089,256.0	2.355	12.62
15	22.416	3922	187,208,352	139,093,152.0	7.782	41.71

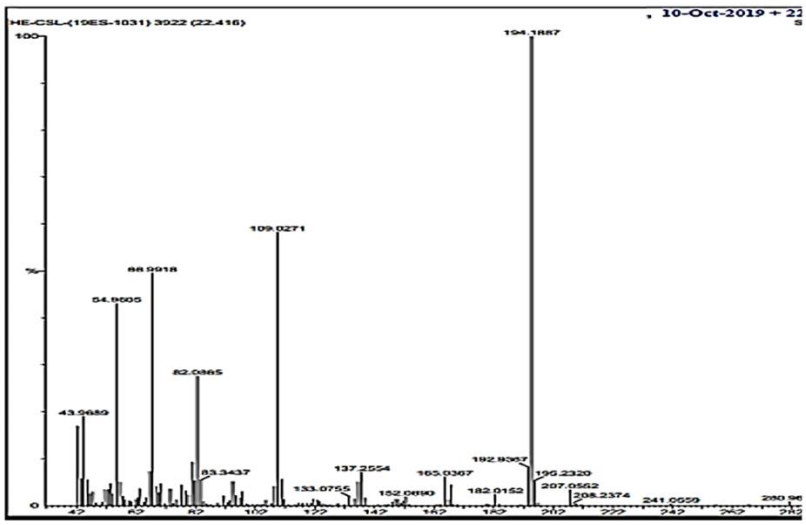

Figure 21: GC-MS profile of the selected chromatographic fraction of *Camellia sinensis* extract

The table and figure reveal that the GC-MS chromatogram of the selected chromatographic fraction of the hydroethanolic extract of *Camellia sinensis* included a

complex mixture of flavonoids and caffeine. Compared with other components *Camellia sinensis* extract possess highest peak range, which is denoted by the presence of flavonoids in the hydroethanolic extract of *Camellia sinensis.*

Similar findings were observed by Hasan *et al.,* (2024) who inferred that the GC-MS profiling of *Camellia sinensis* reveals the presence of eight compounds with caffeine having a retention time 27.44 and yield of 74.47%. Another study by Valli and Divya. (2019) reported that the GC-MS analysis of the ethanolic extract of *Camellia sinensis* leaves had squalene, tetracosane, ascorbic acid and stigmasterol. The above results are supported by Moldoveanu, (2014) who emphasized that the GC-MS profiling of silylated green tea dry leaf extract exhibited catechin and caffeine peaks at retention time of 64.32 and 37.79 respectively.

Thus it can be inferred from the above findings that the selected chromatographic fraction of the hydroethanolic extract of *Camellia sinensis* had flavonoid compounds as confirmed by the GC-MS profile.

4.2.6.7. Results of NMR of the selected chromatographic fraction of *Camellia sinensis* extract

NMR is an effective technique that is capable of monitoring any type of chemical compound containing the element hydrogen in a single experiment. It detects the molecular structure of an element at the atomic level (Zhao *et al.,* 2020).

Figure 22 illustrates the quantitative NMR spectrum of the selected chromatographic fraction of the hydroethanolic extract of *Camellia sinensis*

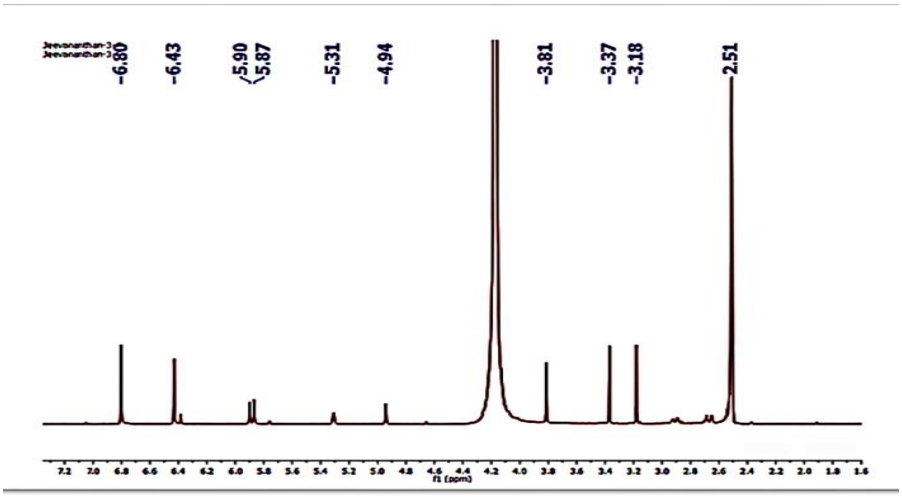

Figure 22: NMR spectrum of the selected chromatographic fraction of *Camellia sinensis* extract

It is revealed from the above figure that the NMR spectrum of the selected chromatographic fraction of the hydroethanolic extract of *Camellia sinensis* indicated the presence of flavonoids and caffeine. The ^{1}H NMR spectra of tea polysaccharides revealed the presence of repeating monosaccharide and disaccharide units from 2.51-6.80 ppm. The NMR peak at δ 4.94 revealed the presence of galactose followed by a peak at δ 5.31-5.87 which revealed the presence of arabinose and a peak at δ 5.9 ppm which revealed the presence of rhamnose. Hence, the abovet results confirmed the presence of polysaccharides made up of mono sugars and repeating mono and disaccharide units in the sample analysed.

In tune with the present study, the reports of a study on tea leaves by NMR spectroscopy highlighted the presence of metabolites such as caffeine, sugars such as sucrose and glucose (Mozumder *et al*., 2020). Another NMR study by the same scientist and team on two varieties of green tea reported the presence of catechin, epigallocatechingallate, gallocatechin, catechingallate and sugars including glucose. A work by Wahyuni *et al*., (2017) also stated the presence of phenols, sugars and derivatives of catechin in three varieties of green tea leaves.

The above finding confirms the presence of polysaccharides made up of mono sugars and repeating mono and disaccharide units in *Camellia sinensis.*

4.2.6.8. Results of LC-MS of the selected chromatographic fraction of *Camellia sinensis* extract

Liquid Chromatography-Mass Spectrometry/ tandem Mass Spectrometry (LC-MS/MS) is used to identify bioactive components, characterize the chemical structure, molecular mass, fragmentation information, retention time and accomplish a broad range of detection and separation of analytical chemicals (Riswanto *et al.*, 2022).

The LC-MS spectrum of the selected chromatographic fraction of the hydroethanolic extract of *Camellia sinensis* is depicted in Figure 23.

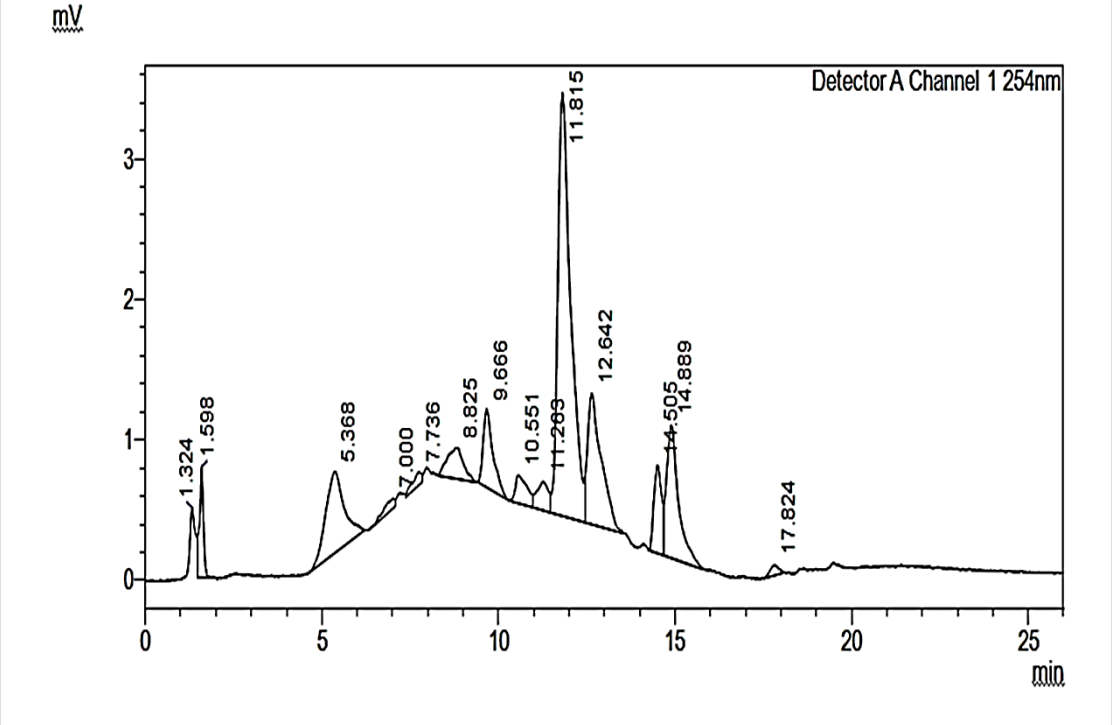

Figure 23: LC-MS Spectrum of the selected chromatographic fraction of *Camellia sinensis* extract

It is evident from the above figure that the sample contains mixed metabolites of gallic acid and catechins in a sequential cleavage maner. The liquid analysis mass peak chromatogram defines that the peak intensity of the target compound was clearly exhibited at the range of 280 nm and represents at m /z from 7.0042 to 8.992. The MS peak represented at 1.324 shows the presence of gallic acid (GA), followed by mass at 5.36 denotes the epigallocatechin (EGA), 7.00 represents the presence of epicatechin (EC), 7.73 revealed that epigallocatechingallate (EGCG), 8.82 revealed the presence of epicatechingallate (ECG) and the peak at 8.85 revealed the presence of catechingallate (CG). The mass spectrum data contains additional signals which clearly indicates the occurrence of caffeine and its derivatives.

Hence, this study strongly suggested the presence of functional metabolites in *Camellia sinensis* leaves.

The above results are in accordance with the reports of (Susanti *et al.*, 2015) who concluded that identification of a cloned green tea variety (GMB-4) by LC MS revealed the presence of major compounds such as epicatechingallate, epigallocatechin gallate, epigallocatechin and epicatechin. The present results are also supported by the work of Tariq

et al., (2015) who stated the presence of polyphenolic catechins in the ethanolic extract of green tea. Another study by Matei *et al.*,(2015) also concluded the presence of a peakof catechin from the ethanol extract of a medicinal plant. In another study, a total of 24 flavonoid derivatives consisting of mainly catechins, flavonols and theaflavins were separated and identified in green and black tea leaves (Lee *et al.,* 2019).

Hence, the presence of functional metabolites (gallic acid, epigallocatechin, epicatechin, epigallocatechingallate, epicatechingallate and catechingallate) in *Camellia sinensis* leaves is confirmed.

Thus from the overall results of Phase II, it can be concluded that *Camellia sinensis* leaves contain a good amount of antioxidants and radical scavenging activity and the main active component present is catechin.

The next phase is focused on the zinc oxide nanoprticle synthesis using *Camellia sinensis* leaf extract and then capped on the catechin. The catechins has a major role in the study as a reducing and capping agent of nanoparticle synthesis.

4.3. Phase III

Characterization of synthesized zinc oxide nanoparticles from *Camellia sinensis*

This phase aimed at synthesizing zinc oxide nanoparticles from the aqueous leaf extract of *Camellia sinensis*. The synthesized zinc oxide nanoparticles were characterized by UV-visible spectroscopy, Scanning Electron Microscopy (SEM), X-Ray diffraction, Fourier Transform Infra Red Spectroscopy (FTIR), zeta potential and also acetylcholine esterase inhibitory activity and antioxidant activities.

4.3.1. Characterization of synthesized zinc oxide nanoparticles from *Camellia sinensis*

4.3.1.1. Visual observation of synthesized zinc oxide nanoparticles

Table XIV and Plate 3 represent the visual colour change durig the process of synthesis of zinc oxide nanoparticles.

Table XIV

Change in colour of solution during formation of synthesized zinc oxide nanoparticles from *Camellia sinensis*

Sample	Before colour reduction	After colour reduction	Colour intensity	Time
***Camellia sinensis* extract**	Light brown	-	-	-
200 mM zinc acetate	Transparent	Pale yellow	+	Immediate
		Yellowish white	++	After 6 h
		White	+++	After 24 h

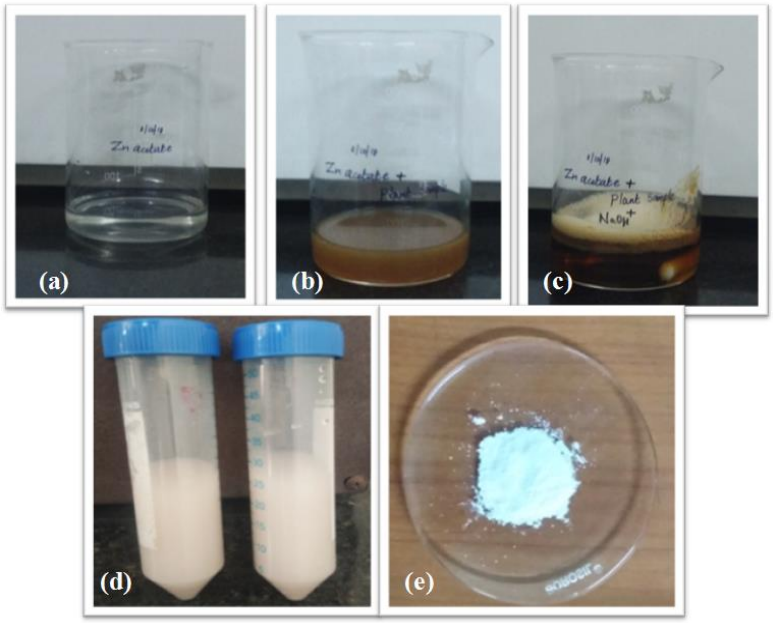

Plate 3: Change in colour of solution during formation of synthesized zinc oxide nanoparticles from *Camellia sinensis*

a) 200 mM zinc acetate solution (transparent) **b) 35 ml of zinc acetate solution + 15 ml of leaf extract (yellowish white)**
c) After 6 h (pale yellow colour) **d) After 24 h (white color, intensity increased)**
e) Synthesized zinc oxide nanoparticles (white powder)

From the table and plate, it can be clearly observed that the colour change of the reaction mixture from transparent to pale yellow occurred after 6 hours and then to white after 24 hours respectively synthesis of zinc oxide nanoparticles from freshly prepared *Camellia sinensis* leaf extract and this is due to the reduction of zinc.

It was also noticed that the white colour was more intense than the preceeding colours of the solution. These observations agree with the results of Kumar *et al.*, (2023)

who also stated that the synthesized ZnO NPs from *Camellia sinensis* were white in colour. The findings are also supported by the work of Fakhari *et al.* (2019), who emphasized that the white colour of the nanoparticles is due to the polyphenols present in the green tea leaf extract, which covers their surface.

It can thus be inferred from the table and figure that a colour change from transparent to white colour occurred on treatment of the *Camellia sinensis* extract with zinc acetate solution confirming the presence of synthesized zinc oxide nanoparticles.

4.3.1.2. Ultra Visible spectrum analysis of synthesized zinc oxide nanoparticles

UV-VIS spectroscopy was used to determine the exact quantities of conjugation, polynuclear compounds and functional groups present in the synthesized zinc oxide nanoparticles from *Camellia sinensis* extract by comparing the results with the standard. (Mohammed, 2018; Rani *et al.*, 2016).

Figure 24 depicts the UV-visible spectrrum of synthesized zinc oxide nanoparticles from *Camellia sinensis*.

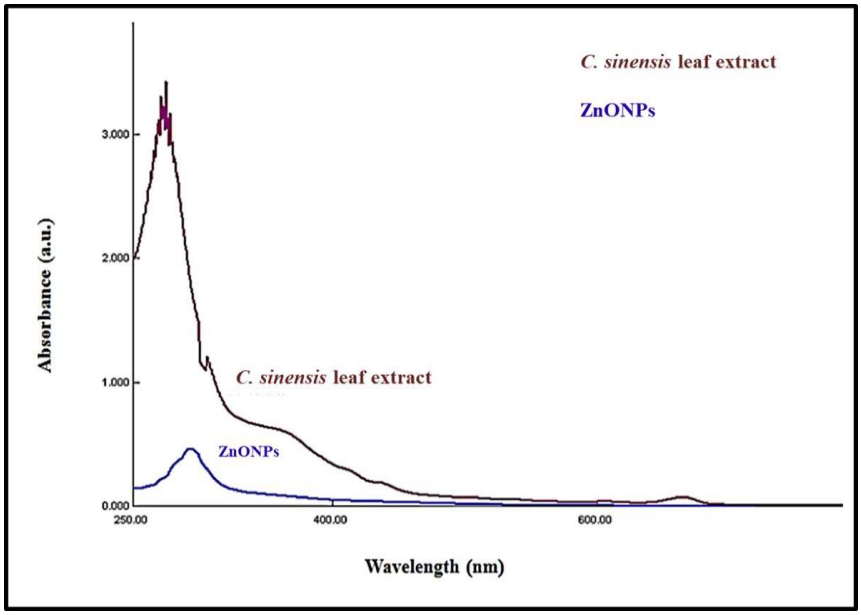

Figure 24: The UV-Visible spectrum of synthesized zinc oxide nanoparticles from *Camellia sinensis*

It is seen from the figure that the spectrum showed a broad peak at wavelength 318 nm which matched with the peak of the zinc oxide nanoparticles. This can be attributed to the intrinsic band gap absorption of zinc oxide nanoparticles due to the electron transition

from the valence band to the conduction band. The band energy of the synthesized zinc oxide nanoparticles was found to be 3.38 eV. The plant extract not only acts as reducing agents but as stabilizing agents as well.

A broad peak at 318 nm as reported in the present study is in accordance with the study of Nagajyothi *et al*., (2015) who made an attempt to synthesize zinc oxide nanoparticles from *Polygala tenuifolia* a herb which showed a broad peak at 314nm. Another study conducted by Dhanemozhi *et al*., (2017) on zinc oxide nanoparticles synthesized from green tea leaves reported a maximum UV absorption spectrum at 338 nm. The results of Sutradhar and Saha, (2015) also stated maximum absorption of zinc oxide nanoparticles from green tea leaf extract at 345 nm.

A broad UV spectrum peak at 318 nm confirms the presence of synthesized zinc oxide nanoparticles from *Camellia sinensis*.

4.3.1.3. Surface topography analysis of synthesized zinc oxide nanoparticles from *Camellia sinensis* using Scanning Electron Microscopy (SEM)

The characterization of nanoparticles can be achieved by the widespread usage of Scanning Electron Microscopy (SEM). Electron-sample interactions yield signals that provide details about the sample, such as its chemical composition, surface appearance or roughness, shape and size of nanoparticles.

Figure 25 illustrates the SEM image of synthesized zinc oxide nanoparticles from *Camellia sinensis* and Figure 26 shows the EDAX spectrum of the synthesized zinc oxide nanoparticles from *Camellia sinensis*

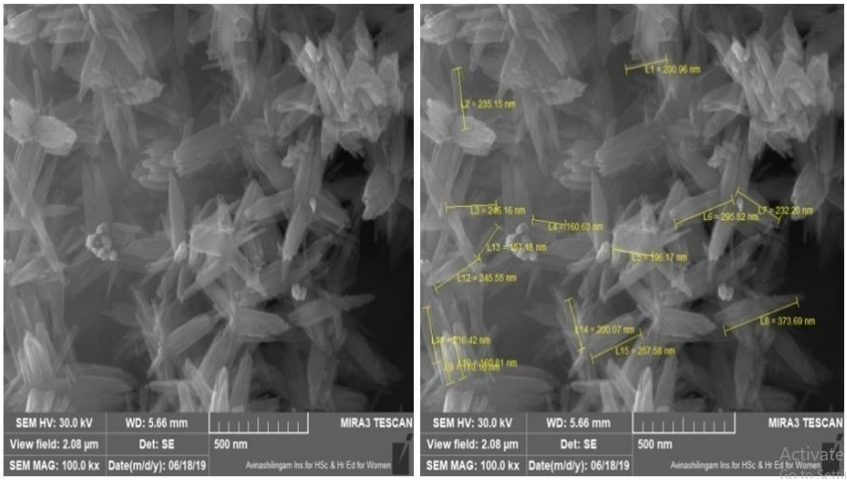

Figure 25: SEM images of synthesized zinc oxide nanoparticles from *Camellia sinensis*

It is understood from Figure 25 that the SEM images under various magnifications (2 µm-200 µm) clearly show the presence of distinct and abundant rod shaped crystals of the synthesized zinc oxide nanoparticles.

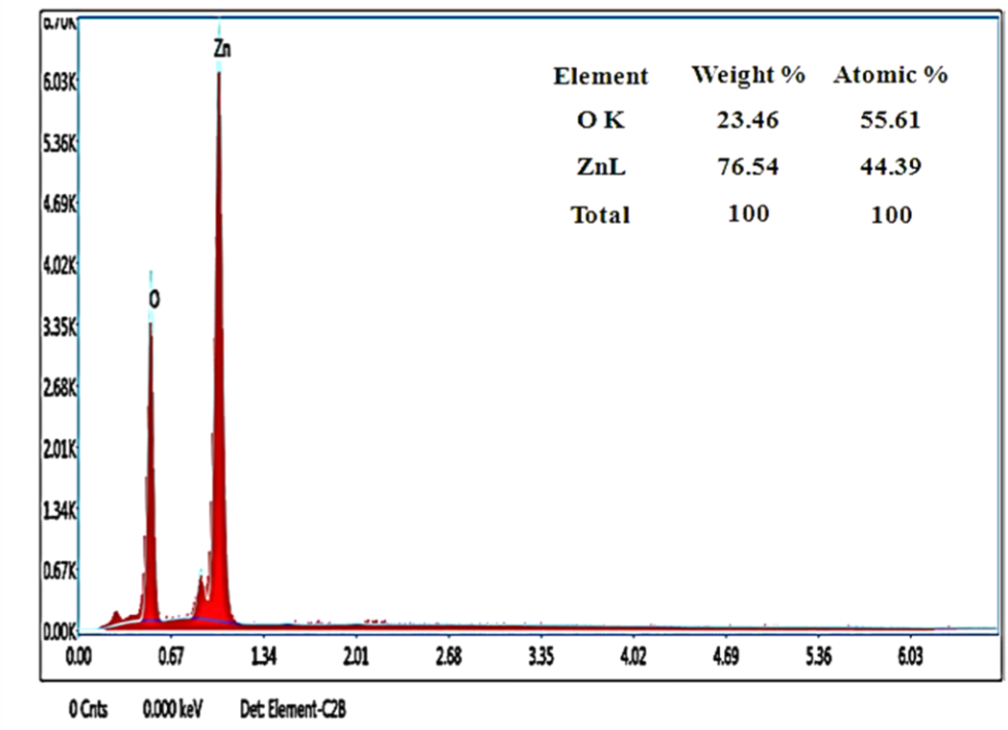

Figure 26: EDAX spectrum of synthesized zinc oxide nanoparticles from *Camellia sinensis*

From Figure 26 it can be noticed that the composition of the elements obtained from EDAX analysis reveals the weight percent value of zinc to be 76.54 % and oxygen to be 23.36 %. The Zn and O showed atomic percent value of 55.61 % and 44.39 % respectively.

The observation of this study reporting the appearance of zinc oxide nonoparticles as rod shaped crystals is similair to the report by Rajeshkumar *et al.*, (2018) who stated that zinc oxide nanopaticles showed agglomerate structures. In agreement with our work is that of Sattar *et al*., (2023) who synthesized zinc oxide nanoparticles from green tea leaves. The pure form of zinc oxide nanoparticles is confirmed by the presence of zinc and oxygen in the green tea extract. Zinc and oxygen have weight percentages of 47.17 and 52.83 and atomic percentages of 78.49 and 21.51 respectively.

It can thus be deduced from the SEM images that the rod shaped crystals confirm the presence of synthesized zinc oxide nanoparticles from *Camellia sinensis.*

4.3.1.4. Elemental mapping analysis of synthesized zinc oxide nanoparticles from *Camellia sinensis*

Analysis of the elements present in the nanoparticles synthesized zinc oxide nanoparticles from *Camellia sinensis* using elemental mapping was carried out, to ensure that the sample contained only zinc and oxygen.

Figure 27 illustrates the results for this.

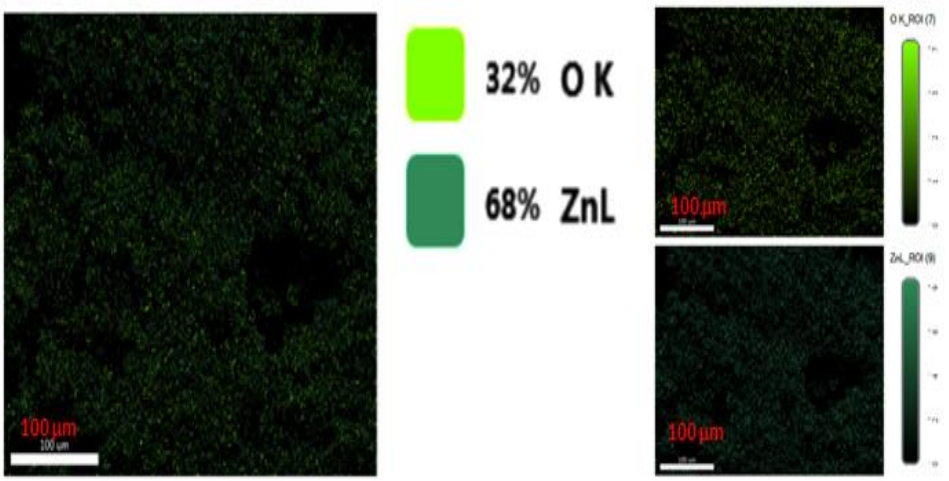

Figure 27: Elemental mapping analysis of synthesized zinc oxide nanoparticles from *Camellia sinensis*

It can be seen from the figure that 68% of the elemental composion of the sample was zinc and 32% oxygen. This confirms that the synthesized zinc oxide nanoparticles were impurity-free and could be observed in the limit of Energy-dispersive X-ray analysis

Similar results were also noted by Jayachandran *et al*. (2021), who found a strong signal for oxygen and zinc after synthesising zinc oxide nanoparticles from aqueous Birdfoot vine leaf extract which indicated that the nanoparticles were pure because it contained only zinc and oxygen. Another observation was stated by Mathizhagan *et al*., (2022) who synthesized zinc oxide nanoparticles from green tea waste and found that elements such as zinc and oxygen which were identified in the sample represent the purity which was confirmed by Energy-dispersive X-ray analysis.

It can be stated from the above finding that the synthesized zinc oxide nanoparticles from *Camellia sinensis* had the elements - zinc and oxygen only thus confirming the purity of the sample.

4.3.1.5. Results of X-ray diffraction studies of the synthesized zinc oxide nanoparticles from *camellia sinensis*

X-ray powder diffraction (XRD) is a strong technique for identifying and measuring the structural parameters (strain state, grain size, epitaxy, phase composition, preferred orientation and defect structure) of crystalline phases in materials.The XRD pattern of ZnONPs was recorded using powder X-ray diffractometer, which provides an insight into the crystallinity of nanoparticles.

Figure 28 shows the XRD diffractogram of the synthesized zinc oxide nanoparticles from *Camellia sinensis.*

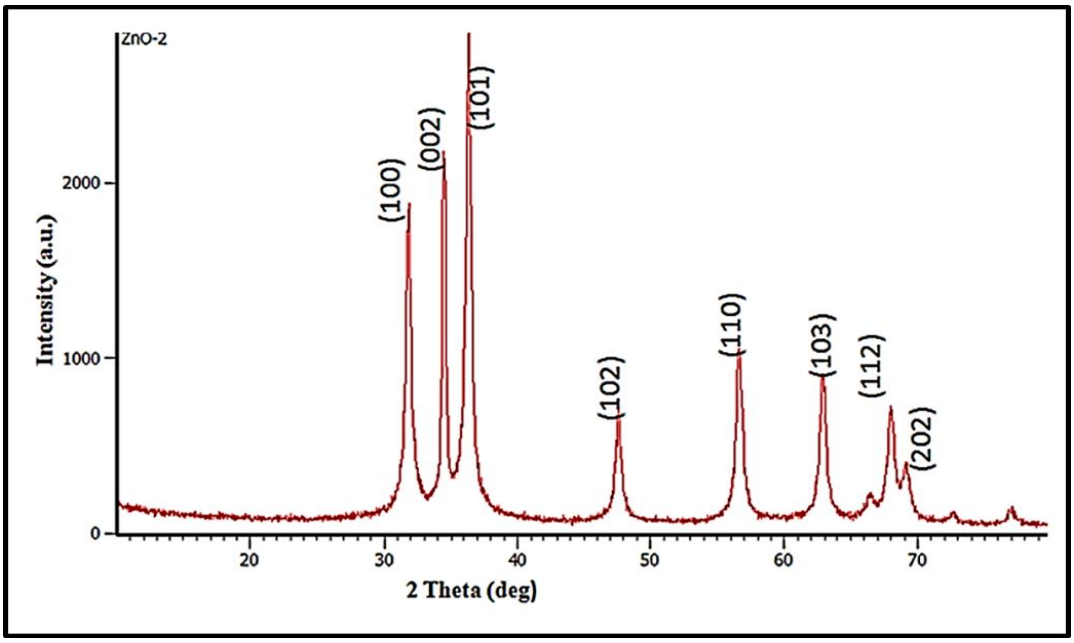

Figure 28: XRD image of synthesized zinc oxide nanoparticles from *Camellia sinensis*

From the figure it can be noted that the XRD of the synthesized zinc oxide nanoparticles was carried out with Cu – κα radiation (κ – 0.154nm) and 2 theta range from 20˚ to 80˚. The image showed 8 strong Bragg reflection peaks (2^{θ} = 31.8˚,34.4˚,36.3˚,47.6˚, 56.6˚,62.9˚,66.4˚ and 77.0˚) which matched with their miller indices ((100), (002), (101), (102), (110), (103), (112) and (202)) obtained from JCPDS card No: 36-1451 (Madathil *et al.*,2007) and with JCPDS card No: 89-7102 (Rajiv *et al.*,(2013) and Selvarajan and Mohanasrinivasan, (2013). From this, the structure of the synthesised zinc oxide nanoparticles was confirmed and found to be wurtzite (hexagonal phase). The size of the synthesised zinc oxide nanoparticles was also found to be 160 nm indicating its crystalline nature.

Similar results were obtained by Sood *et al*., (2023), who synthesized zinc nanoparticles using *Centella asiatica* (Vallarai in tamil) ethanol extract and found the major peaks of 2θ values were 31.66°, 34.36°, 36.23°, 47.45°, 56.47°, 62.90°, 67.92° and 69.08°. The X-ray diffraction peaks of bush tea showed peaks at (100),(002),(110),(100),(103), (201),(112),(201), (004),(202) are lattice planes which comfirmed that the synthesized zinc oxide nanoparticles were crystalline in structure (Kaningini *et al*., 2022). Another study carried out by Irshad, *et al* (2018) reported that the XRD diffraction pattern of Zinc oxide nanoparticles from green tea leaves showed major peaks of 2θ values from 20 to 70 ((100), (002), (101), (102), (110) and (112)).

The diffractogram of the sample studied proved the synthesized zinc oxide nanoparticles to be crystalline in nature with the size of 60 nm.

4.3.1.6. Functional group analysis of the synthesized zinc oxide nanoparticles from *Camellia sinensis* using Fourier Transform Infra-Red (FTIR) spectroscopy

Fourier Transform InfraRed spectroscopy (FT-IR spectroscopy) has been employed to identify the biomolecules found *Camellia sinensis* plant extracts that are responsible for green synthesis of nanoparticles and their stabilization and reduction processes. Substance-specific vibrations of the molecules lead to the specific signals obtained by IR spectra.

Figure 29 represents the FTIR spectra of synthesized zinc oxide nanoparticles from *Camellia sinensis.*\

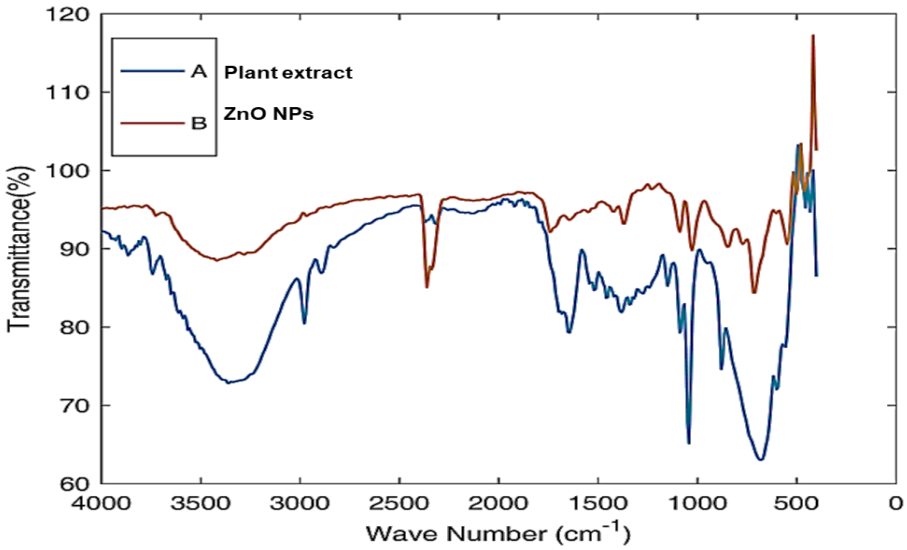

Figure 29: FT-IR spectra of synthesized zinc oxide nanoparticles from *Camellia sinensis*

From the figure it can be expressed that the FT-IR spectra of *Camellia sinensis* leaf extract before nanoparticle synthesis gave an absorption band at 3390-3228 cm^{-1} representing O-H stretching alcohol and carboxylic acid. The absorption peak located at around 2773 cm^{-1} represented –O-H stretching carboxylic acid stretching vibrations present at 1643 and 1701 cm^{-1} are associated with C=O stretch vibration of amides and aldehydes respectively. The strong absorption peak at 1361 is assigned to CH $(CH_3)_2$ stretching alkanes and alkyls 1226 $cm^{-1}$to and =C-O- sym and asym stretch ethers. Small bands at 1504, 929 and 821cm-1 represent N-H stretching amides, =C-H- stretching alkanes and C-H stretching vibration of aromatic compounds respectively.

After the synthesis of zinc oxide nanoparticles, the FT-IR spectra showed (Figure 29) strong absorption peaks at 3441, 2300, 1366, 1026 and 709 cm^{-1} which were assigned to –N-H- stretching amines symmetric and aymmetric –O-H- stretching carboxylic acids, CH3-C-H stretching alkanes and alkyls, C-O stretching alcohol and C-H stretching aromatic compounds respectively. The weaker bands at 1419, 1087, 848 and 547cm^{-1}correspond to aromatic compounds (-C-C- stretching), alcohol (C-O- stretching), alkenes (=C-H- stretching) and alkyl halides (C-Br- stretching) respectively. The band at 463 cm^{-1}confirms stretching vibration of zinc oxide nanoparticles.

Similar findings as above were reported by Abdelbaky *et al.,* (2023) who compared the FTIR spectrum of lemon grass water extract and synthesized zinc oxide nanoparticles from lemon grass. Both the spectra showed similar types of stretching such as amides, aldehydes, aromatic ring and amino acids. The broad peak at 435.83 nm indicates the presence of zinc oxide in lemon grass extract contains ZnONP. Nagajyothi *et al.,* (2015) compared the FTIR spectrum of *Polygala tenuifolia* root extract (an herb) and Zinc oxide nanoparticles synthesized from *Polygala tenuifolia*. It shows strong absorption peaks at 1075, 1660, 2927, 3380, where 0-H stretching indicates alcohols and phenols, C-H stretching alkanes, C-N stretching aliphatic amines and C-H stretching alkanes. Yet another report given by Jamdagni *et al.*,(2018), mentioned that the FTIR spectrum of synthesized zinc oxide nanoparticles from Night jasmine gave peaks at 3340.6 and 3258.2 indicating (H-OH stretch and N-H stretch), N-H stretching (amines) respectively.

Thus from the above results it can be deduced that the synthesised zinc oxide nanoparticles from *Camellia sinensis* contains the functional groups amines, carboxylic

acids, alkanes, alkyls and alkyl halides. The peak at 463 cm^{-1} is assigned to Zn-O stretching vibrational mode of zinc oxide nanoparticles.

4.3.1.7. Surface Charge of the synthesized zinc oxide nanoparticles from *Camellia sinensis* using zeta potential

Zeta potential was used to determine the surface potential of the synthesized zinc oxide nanoparticles and it is an essential characterization for stability in zinc oxide nanoparticles. The zeta potential may either have high negative value or high positive value which makes them repel each other and prevent them from agglomeration. On the other hand, the low negative and positive zeta potential indicates that the particles are highly prone to agglomeration. This high negative or positive zeta potential provides long term stability to the particles (Sharma *et al.*, 2022).

Figure 30 reveals the zeta potential of synthesized zinc oxide nanoparticles from *Camellia sinensis.*

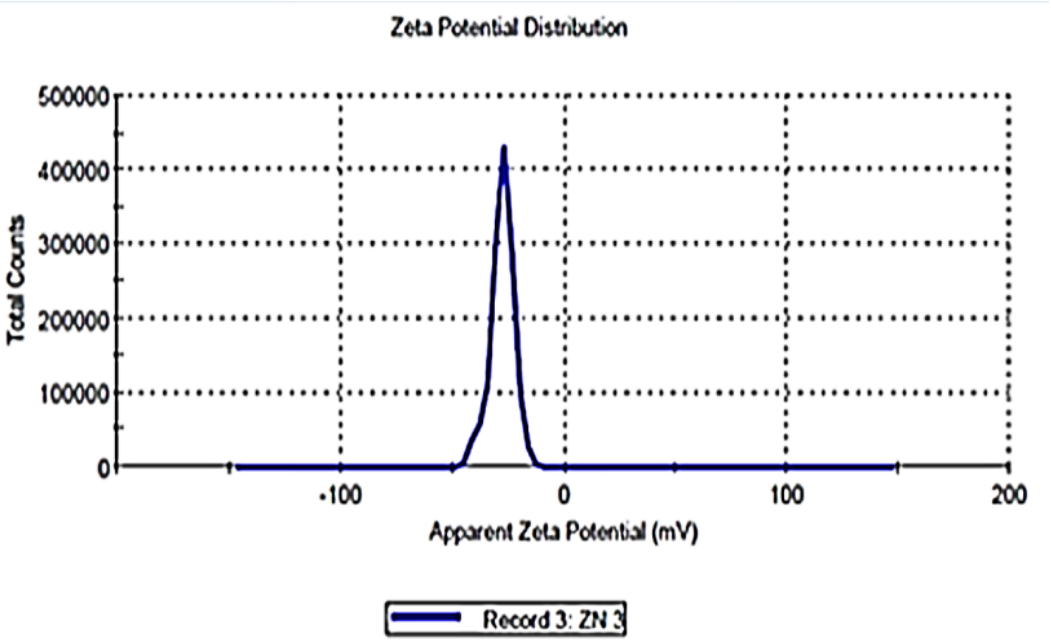

Figure 30: The Zeta potential of synthesized zinc oxide nanoparticles from *camellia sinensis*

A minimum of +30 mV to -30 mV zeta potential is required for the indication of stable synthesized zinc oxide nanoparticles. In the above figure the synthesized zinc oxide nanoparticles had a zeta value of -11.6 mV with a peak area of 100 % intensity proving that the synthesized zinc oxide nanoparticles were stable.

Similar findings as above were observed by Jan *et al.*, (2021) who synthesized zinc oxide nanoparticles from the leaf extract of Himalayan columbine, a flowering herbaceous perennial plant and observed that the zeta potential value of the zinc oxide nanoparticles was found to be -18.4 mV proving diffusion stability and prevention of accumulations of the nanoparticles. Other findings were indicated by Wang *et al.*, (2022) and Sohail *et al.*, (2020) who synthesized zinc oxide nanoparticles from coffee leaf extract and neem leaf extract and observed the zeta potential value to be -23.84 and -23.6 respectively.

The zeta value confirmed the stability of the synthesized zinc oxide nanoparticles from *Camellia sinensis* proving them to be suitable for capping with catechin.

4.3.2. Antioxidant activity of synthesized zinc oxide nanoparticles from *Camellia sinensis*

The antioxidant activity of the synthesized zinc oxide nanoparticles was measured using DPPH radical scavenging activity.

The results of the DPPH radical scavenging activity in the synthesized zinc oxide nanoparticles from *Camellia sinensis* is depicted in Figure 31.

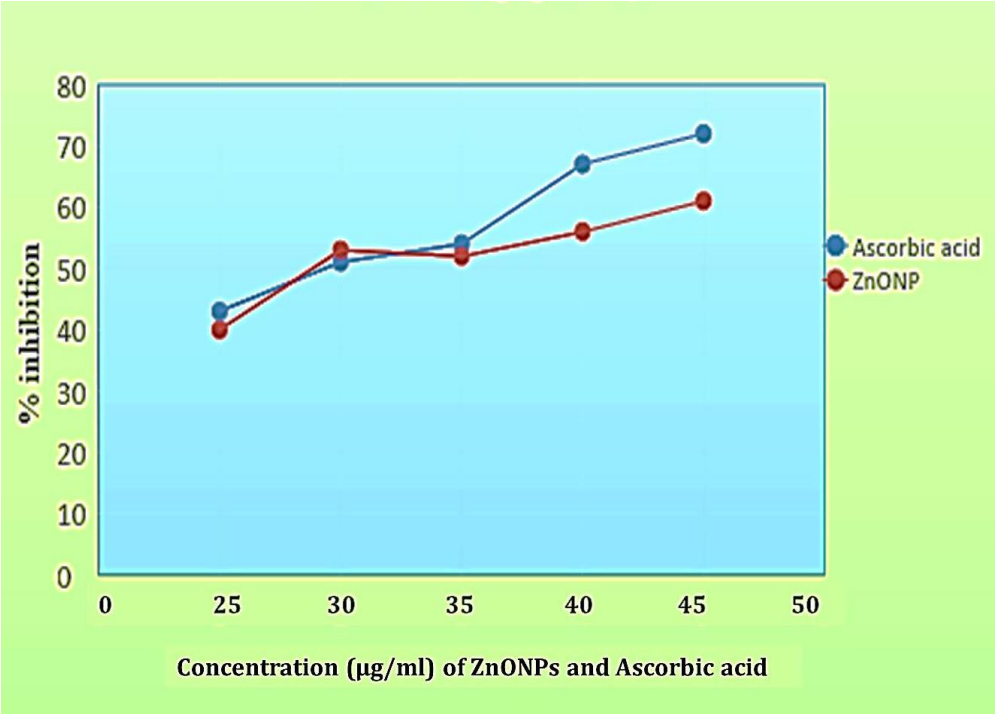

Figure 31: DPPH scavenging activity of synthesized zinc oxide nanoparticles from *Camellia sinensis*

It can be noticed from the figure that the percent inhibition of scavenging activity of the synthesized zinc oxide nanoparticles increased in a dose dependent manner which was comparable to that of standard at the same concentration. The IC_{50} value of the synthesized zinc oxide nanoparticles was found to be 70.37 %.

The increase in the percent inhibition of scavenging activity of the synthesized zinc oxide nanoparticles in a dose dependent manner is similar to the results of Alahdal *et al.*,(2022) and Chatterjee *et al* (2023), who stated that the antioxidant activity of zinc oxide nanoparticles of the *Phragmanthera austroarabica* (semi parasitic plant) leaf extract and chamomile tea (a type of green tea) extract, showed an increase percentage inhibition with increase concentration. A related study was carried out by Jan *et al.,* (2021), who stated that the highest antioxidant activity was observed in zinc oxide nanoparticles from aqueous leaf extract of *Aquilegia pubiflora* (Himalayan Columbine - medicinal plant).

Thus, it can be concluded from the above findings that with increase in the concentration of zinc oxide nanoparticles, the antioxidant activity increased.

4.3.3. Neuroprotective effect of synthesized zinc oxide nanoparticles from *Camellia sinensis*

4.3.3.1. Results of Thin Layer Chromatography (TLC) with bioassay detection for AChE inhibition

TLC of the synthesized zinc oxide nanoparticles from *Camellia sinensis* was carried out. From the results it is clearly understood that the synthesized zinc oxide nanoparticles from *Camellia sinensis* showed the presence of a single spot with Rf value of 0.63. The spot appeared white in colour against a yellow background indicating the presence of acetyl cholinesterase.

A study by Trevisan *et al.*, (2006) mentioned that TLC of *Kalanchoe brasiliensis* (love bush) showed a white spot on chromatogram indicating the inhibitory property of the flavonoid compounds against cholinesterase. Another study by Haddi *et al.*,(2024) reported that TLC bioautography of various extracts of *Pistacia lentiscus* (*mastic tree)* with two controls (ascorbic and quercetin) displayed yellow spots against a purple background when exposed to DPPH indicating the potential of zinc oxide nanoparticles to reduce DPPH radicals.

Hence the presence of white spot on the TLC plate showed the inhibitory property of the synthesized zinc oxide nanoparticles from *Camellia sinensis* against cholinesterase.

4.3.3.2. Acetyl cholinesterase (AChE) inhibitory activity of synthesized zinc oxide nanoparticles from *Camellia sinensis*

Acetylcholinesterase (AChE) inhibitors are used to treat neurological disorder patients because they enhance cholinergic neurotransmission. It is urgent to find new and efficient inhibitors from natural sources, highly bioavailable with low or no toxicity (Ferreira *et al.*, 2020).

Figure 32 represents the Acetyl cholinesterase (AChE) inhibitory activity of synthesized zinc oxide nanoparticles from *Camellia sinensis.*

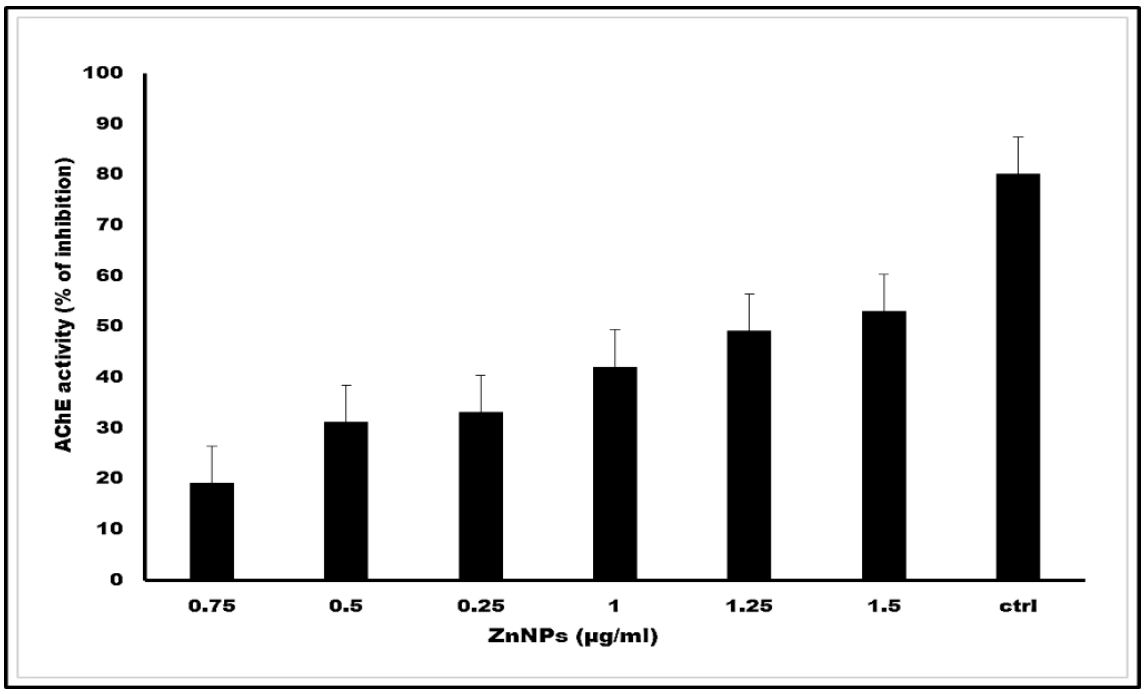

Figure 32: Acetyl cholinesterase (AChE) inhibitory activity of synthesized zinc oxide nanoparticles from *Camellia sinensis*

It is revealed from the figure that the concentration of 1.25 µg/ml of the synthesized zinc oxide nanoparticles showed the most potent effect on acetylcholinesterase inhibition activity. When studied for its inhibitory effect on the synthesized zinc oxide nanoparticles, acetylcholinesterase was found to cause the inhibition in a dose dependent manner 0.75, 0.50, 0.25, 1, 1.25 and 1.5 µg/ml of synthesized zinc oxide nanoparticles.

The present study agrees with the results of Feitosa *et al.,* (2011) who reported that a mixture of plant extracts showed maximum inhibition of acetylcholinesterase activity provig that the extracts could be successfully used to treat the symptoms of Alzheimer's disease.

This result proved that the synthesized zinc oxide nanoparticles from *Camellia sinensis* had a potent acetylcholinesterase inhibition activity

From the overall findings of Phase III it can be concluded that there is a good potential for the synthesized zinc oxide nanoparticles from *Camellia sinensis* to be a valuable source of antioxidants with acetylcholinesterase inhibitory activity.

4.4. Phase IV:

4.5. Synthesized zinc oxide nanoparticle-capped catechin their characterization and *in vitro* neuroprotective activity

Synthesized zinc oxide nanoprticles from *Camellia sinensis* were used to cap the isolated active constituent catechin from green tea extract by encapsulation (nano precipitation method). The crystal structures, optical and morphological features of the synthesized zinc oxide nanoparticle-capped catechin and *in vitro* neuroprotective activity were examined.

4.4.1. Characterization of synthesized zinc oxide nanoparticle-capped catechin

UV visible spectroscopy, Fourier Transformed InfraRed spectroscopy (FTIR), Scanning electron microscopy (SEM), and X-ray powder diffractometry (XRD) and Zeta potential were used to characterize the nanoparticles composition, their shape, size, crystallinity and stability.

4.4.1.1. Results of UV – visible spectrum analysis of synthesized zinc oxide nanoparticle-capped catechin

The initial analytical characterization of the synthesized zinc oxide nanoparticle-capped catechin was done by UV visible spectroscopy and the results are shown in Figure 33.

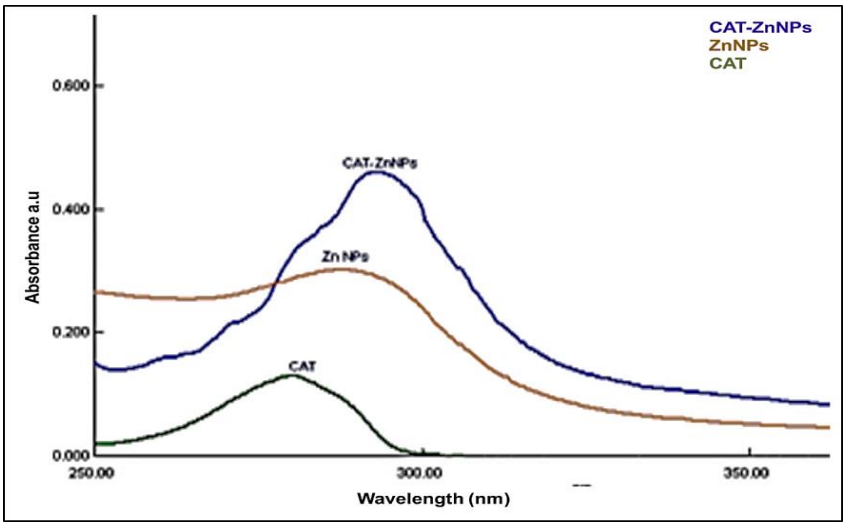

Figure 33: UV-visible spectra of synthesized zinc oxide nanoparticle-capped catechin

It can be seen from the figure that the absorption spectrum of the synthesized zinc oxide nanoparticle-capped catechin showed a broad peak at 318 nm. The reaction proceeded under an ambient temperature of 26°C for 1 hour, and was fast and required minimal energy. The UV absorption of catechin and zinc oxide nanoparticles were observed to be around 260 nm to 280 nm respectively. UV absorption of zinc oxide nanoparticle-capped catechin exhibited a hyperchromic shift at 318 nm range compared to catechin and zinc oxide nanoparticle UV-absorption. This is denots preliminary confirmation of the zinc oxide nanoparticles being coated on the catechin.

Studies by Zhang *et al., (*2014) and Sentkowsa and Pyrzynska, (2023**)** who stated that selenium nanopartilcles conjugated with epigallocatechin-3-gallate and selenium nanopartilcles conjugated with epigallocatechin-3-gallate and coated with Tet-1 peptide gave UV absorbance peaks at 285 and 380 nm respectively. Further, the UV absorption spectrum of catechin functionalized ZnO colloidal solution showed absorption peaks in the range of 330 to 430 nm which matched with the absorption band of the ZnO colloidal solution (Zhao *et al*., 2021).

This result proves that the UV spectrum of the synthesized zinc oxide nanoparticle-capped catechin resulted in a broad peak at 318 nm wavelength.

4.4.1.2. Results of surfaces topography analysis of synthesized zinc oxide nanoparticle-capped catechin by SEM

SEM analysis was carried out to study the morphological characteristics of the synthesized zinc oxide nanoparticle-capped catechin. Further information on the 3D

structure and topography of the nanostructures were obtained. The results are shown in Figure 34.

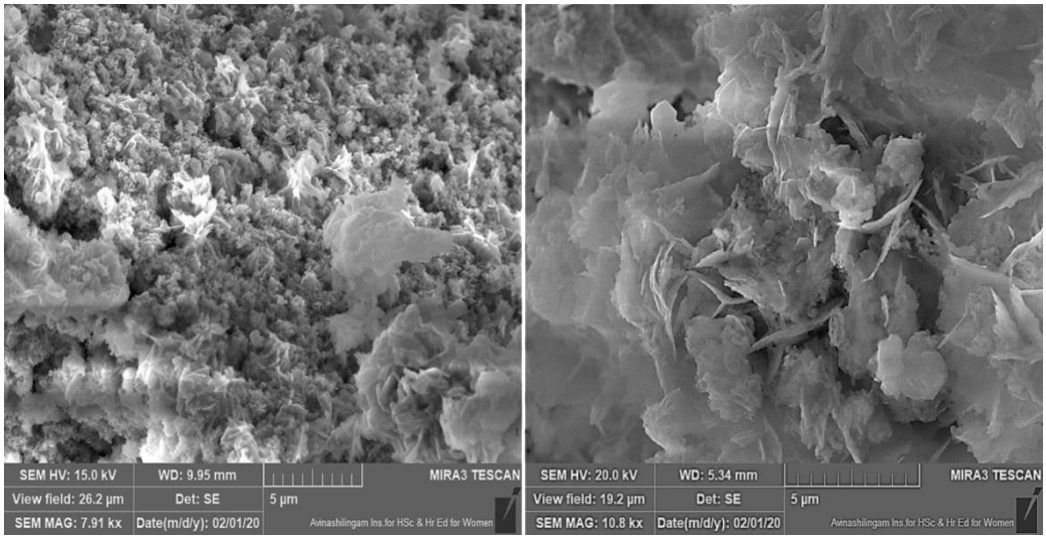

Figure 34: SEM images of synthesized zinc oxide nanoparticle-capped catechin magnification range (5 µm)

From the figure it can be observed that under the magnification of 5 µm, the synthesized zinc oxide nanoparticles from *Camellia sinensis* were completely capped on the catechin with uniform distribution in the solution and they appeared to be rod-shaped. Some of these rod shaped particles which had smooth surface were found to be present as agglomerates.

Similar findings as above were observed by Jeyaleela et al., (2020), who reported that SEM images of biosynthesized quercetin-mediated zinc oxide nanomaterials showed zinc nano fiber type morphology. The study was also supported by Sadhukhan *et al.,* (2019), who had reported that the images obtained from SEM analysis of synthesized phenylboronic acid- conjugated zinc oxide nanoparticles loaded with quercetin were found to have a tetragonal morphology. The results were also in agreement with the work of Arasoglu *et al.,* (2015), who reported that the SEM images of quercetin-loaded polylactic-co-glycolic acid (PLGA) nanoparticles (without solvent) showed morphological changes with hydrophobic characteristics.

Hence the present results clearly indicated that the synthesized zinc oxide nanoparticles completely capped the catechin with uniform distribution which appeared as rod-shaped structures.

4.4.1.3. Analysis of diffractogram of synthesized zinc oxide nanoparticle-capped catechin

The crystalline phases of the synthesized zinc oxide nanoparticle-capped catechin were studied by XRD in relation to the strain state, grain size, epitaxy, phase composition, preferred orientation and defect structure.

Figure 35 records the XRD patterns of synthesized zinc oxide nanoparticle-capped catechin.

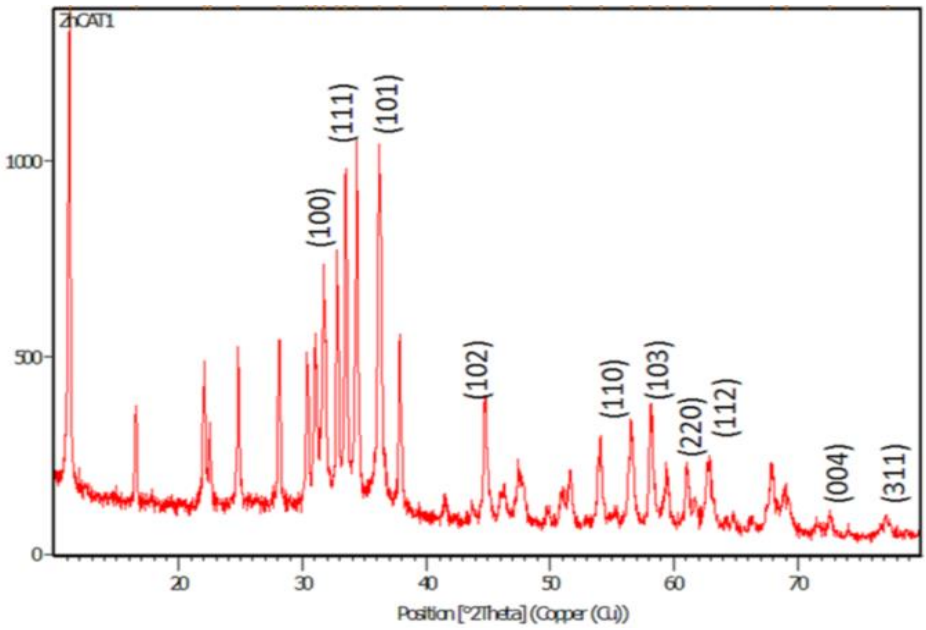

Figure 35: XRD patterns of synthesized zinc oxide nanoparticle-capped catechin

It is understood from the figure that intense diffraction peaks were observed at 2θ value of 31.9°, 34.4°, 36.2°, 45.6°, 56.5°, 58.6°, 61.8°, 63.3°, 73.1 and 78.5° corresponding to the (100), (111), (101), (102), (110), (103), (220), (112), (004) and (311) planes respectively of the face-centered cubic. The predominant orientation was that of the (111) plane, because, the most intense peaks appeared at 34.4° which revealed that the nanoparticles were crystalline in nature with a size of 50-60 nm.

The above results are supported by other researchers like Al-Mosawi*et al.*, (2023) and Kim *et al.*, (2022) who emphasized that XRD studies of starch-based zinc oxide nanoparticles and zinc oxide nanoparticles with and without polyphenols produced diffraction peaks at 2ω values of 31.7°, 34.4°, 36.2°, 47.5°, 56.6°, 62.8°, 66.3°, 67.9°, 98 and

72.5° which corresponded to the orientation planes (100), (002), (101), (102), (110), (103), (200) and (112). A report by Saleemi *et al.*, (2022) also observed that when zinc oxide nanoparticles were capped with rutin, the diffraction peaks were found in the corresponding planes.

Thus from the above results, the crystalline structure of the synthesized zinc oxide nanoparticle-capped catechin was confirmed.

4.4.1.4. FTIR spectrum analysis of synthesized zinc oxide nanoparticle-capped catechin

Synthesized zinc oxide nanoparticle-capped catechin was further characterized by FT-IR to confirm the existence of chemical bonds that are responsible for the stabilization and reduction processes of nanoparticles.

Figure 36 represents the FT-IR spectrum of synthesized zinc oxide nanoparticle-capped catechin.

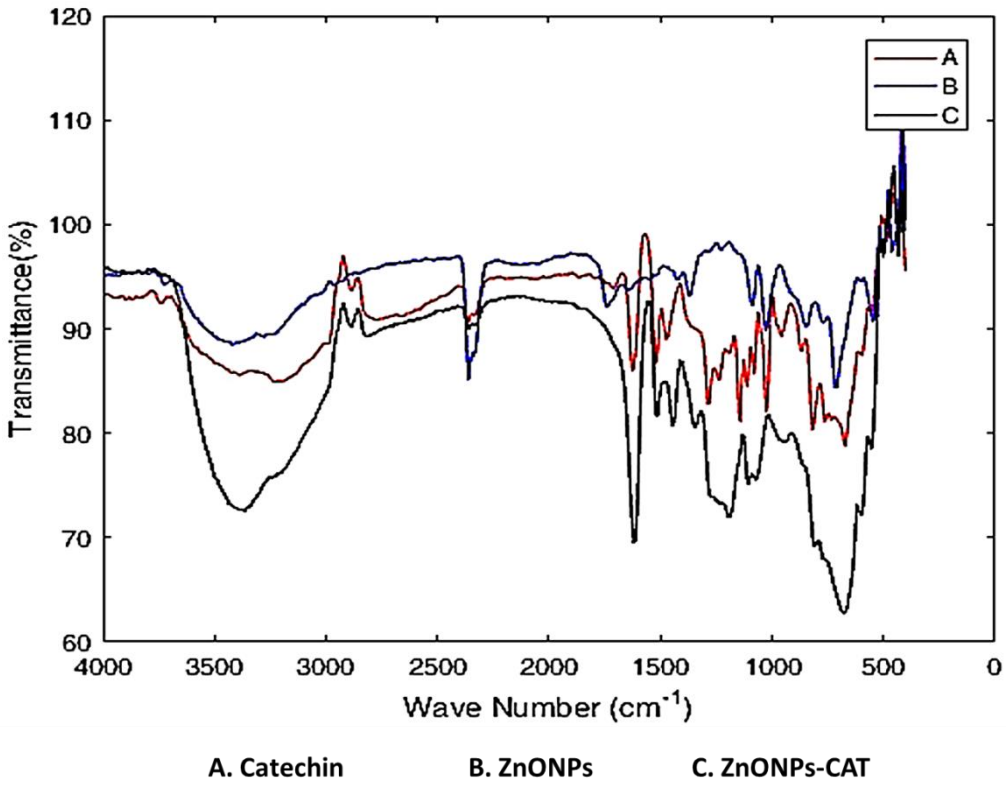

Figure 36: FT-IR spectrum of synthesized zinc oxide nanoparticle-capped catechin

The figure clearly indicates that the FT-IR spectrum of the synthesized zinc oxide nanoparticle-capped catechin showed a broad strong band from 2885 cm^{-1} to 2816 cm^{-1} indicating the presence of OH groups. A medium narrow band at 1620 cm^{-1} was also observed which may be due to the C – O stretch of alcohols. Alongwith this, a weak band at 1442 cm^{-1} was seen due to the in plane bend vibration of OH group. A medium narrow band at 1519 cm^{-1} was due to the presence of –CO– group in the synthesized zinc oxide nanoparticle-capped catechin. The band at 3387 cm^{-1} is due to the –CH=CH – group. FTIR spectrum results showed that the functional groups which were present in the zinc oxide nanoparticles and catechin before capping were also present after capping with no changes.

The above results are in accordance with previous studies. Liu *et al.,* (2018) also reported that the FTIR spectra of catechin-loaded folate conjugated chitosan nanoparticles when compared with the spectra of catechin alone showed the presence of alkenes, carbonyl groups and aromatic rings in both the samples. The results were also similar to that of Chae *et al.,* (2019), who revealed that the FTIR spectrum of lipid - capped zinc oxide nanoparticles exhibited a broad spectrum from 3600 to 3200 cm-1, which can be attributed to the hydroxyl groups present on the surface of the samples. The presence of these peaks explains the successful role of catechin as capping and stabilization agent for synthesized zinc oxide nanoparticles.

Thus the FTIR spectrum showed that the functional groups of the synthesized zinc oxide nanoparticle-capped catechin were retained even after capping without any changes.

4.4.1.5. Results of zeta potential studies on synthesized zinc oxide nanoparticle-capped catechin

The surface potential of the synthesized zinc oxide nanoparticle-capped catechin stability was determined by zeta potential.

Figure 37 depicts the results of the zeta potential of synthesized zinc oxide nanoparticle-capped catechin.

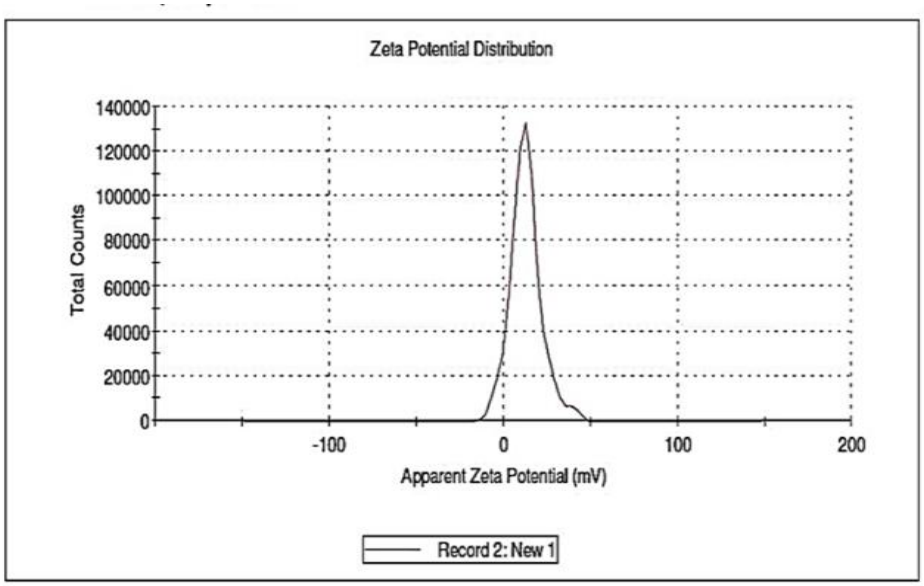

Figure 37: Zeta potential of synthesized zinc oxide nanoparticle-capped catechin

It is evident from the figure that the zeta potential of the synthesized zinc oxide nanoparticle-capped catechin showed a narrow distribution with an average of +11 mV giving a peak area of 100 % intensity conforming that the synthesized zinc oxide nanoparticle-capped catechin are stable.

A similar study as above conducted by Wu *et al.*, (2017) also reported that chitosan-lysozyme nanoparticles had a zeta potential value of 13.6 mV. Another study by Saleemi *et al.*, (2022) also reported zeta potential values of -8.50 and -8.37 mV respectively for standard zinc oxide nanoparticles and synthesized zinc oxide nanoparticles with rutin.

Thus it can confirmed from 2the zeta value that the synthesized zinc oxide nanoparticle-capped catechin are stable.

4.4.2. Antioxidant activity of synthesized zinc oxide nanoparticle-capped catechin

The antioxidant test of the synthesized zinc oxide nanoparticle-capped catechin was measured by 2, 2-diphenyl-1-picrylhydrazyl (DPPH) in order to evaluate its radical scavenging activity.

Figure 38 shows DPPH radical scavenging activity of the synthesized zinc oxide nanoparticle -capped catechin.

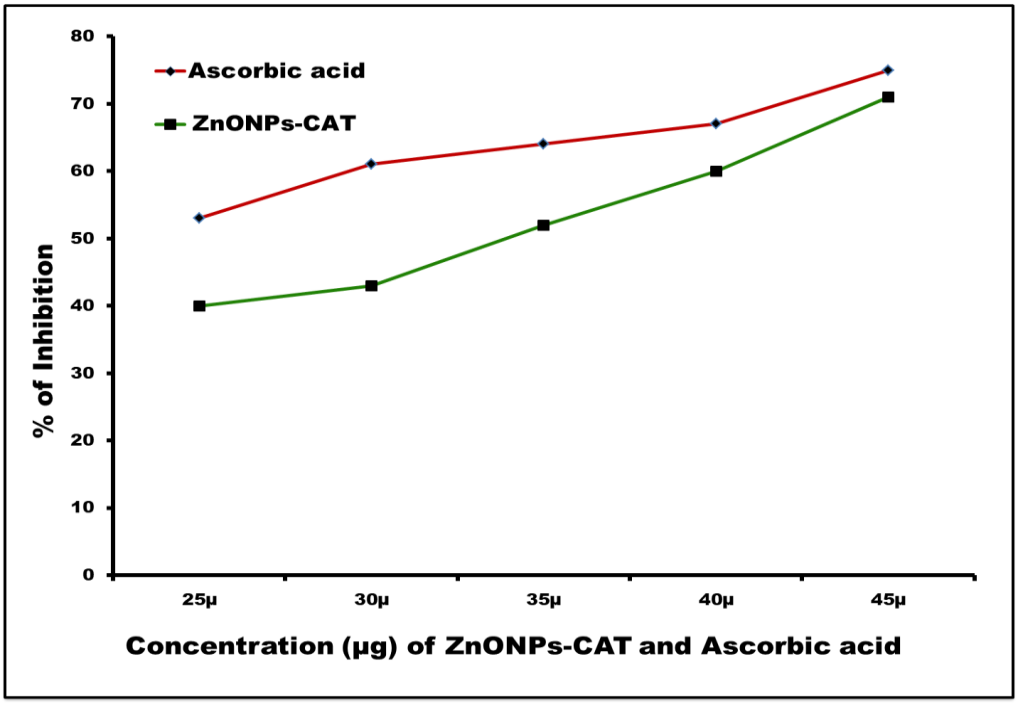

Figure 38: Antioxidant activity of synthesized zinc oxide nanoparticle-capped catechin

It can be observed from the figure that the percent inhibition of scavenging activity of the synthesized zinc oxide nanoparticle-capped catechin was increasing in dose dependent manner which was comparable with that of the standard. The IC_{50} value of the synthesized zinc oxide nanoparticle-capped catechin was determined to be the percent inhibition (52.3 %). Zinc oxide nanoparticle-capped catechin were more effective against radicals and potentially scavenged radicals compared with the standard ascorbic acid.

The above results are supported by Mathew *et al.*, (2012), who emphasized that in attachment of the currcumin- polylactic-co-glycolic acid nanoparticles did not produce any change in its antioxidant activity. The point to be noted is that the capped zinc oxide nanoparticle does not destroy the antioxidant activity of the catechin. Bharathi *et al.*, (2019) on the other hand, reported that synthesised zinc oxide nanoparticles using pure flavonoid rutin had radical scavenging ability.

Hence, the present results clearly indicated that the synthesized zinc oxide nanoparticle-capped catechin had antioxidant activity.

4.4.3. *In vitro* neuroprotective activity of synthesized zinc oxide nanoparticle-capped catechin

The *in vitro* neuroprotective activity of the synthesized zinc oxide nanoparticle-capped catechin was studied by to demonstrate entrapment efficiency and loading capacity, drug release and inhibition of acetylcholinesterase (AChE) activity.

4.4.3.1. Entrapment efficiency and loading capacity of synthesized zinc oxide nanoparticle-capped catechin

Table XV reveals the entrapment efficiency and loading capacity of synthesized zinc oxide nanoparticle-capped catechin

Table XV

Entrapment efficiency of synthesized zinc oxide nanoparticle-capped catechin

Sample	Time (sec)	Homogenization speed (rpm)	Sonication power (W)	Encapsulation efficiency (%)
synthesized zinc oxide nanoparticle-capped catechin	120	24,000	80	78.2

From the table it is obvious that the encapsulated synthesized zinc oxide nanoparticle-capped catechin obtained from nano-precipitation method had 78.2 % encapsulation in 120 seconds at a homogenization speed of 24000 rpm and sonication power of 80 w.

Thus, it can be said that the synthesized zinc oxide nanoparticle-capped catechin is encapsulated

4.4.3.2. Results of *In vitro* release study of synthesized zinc oxide nanoparticle-capped catechin

The solubilities of the drugs in their respective release medium were determined prior to the *in vitro* release study of the synthesized zinc oxide nanoparticle-capped catechin.

The *In vitro* release profiles of optimized synthesized zinc oxide nanoparticle-capped catechin are plotted in Figure 39.

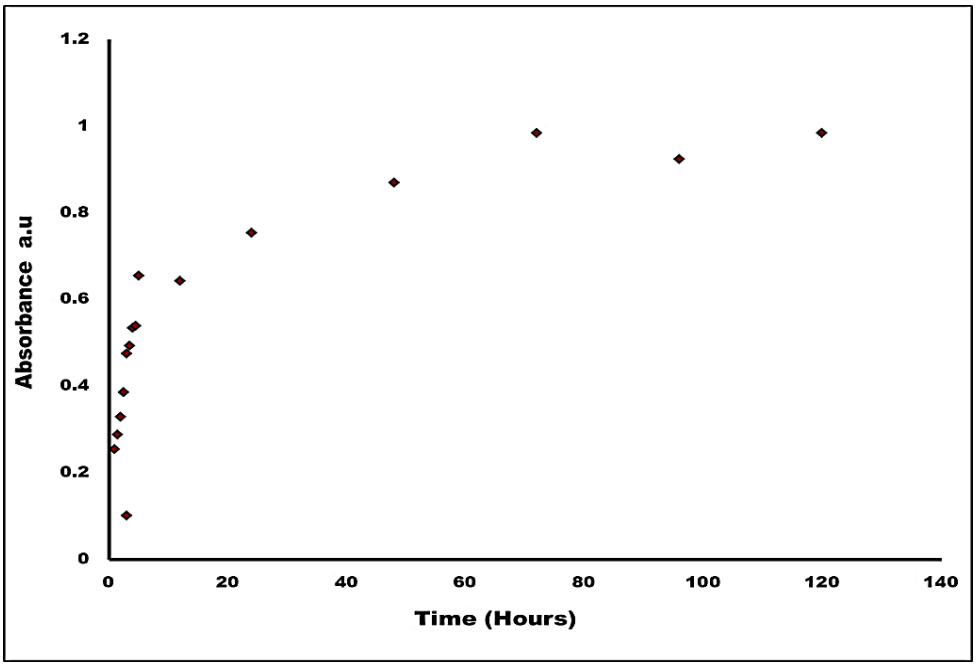

Figure 39: *In vitro* drug release of synthesized zinc oxide nanoparticle-capped catechin

It is understood from the figure a near linear and continuous release was observed over 72-120 hours. The synthesized zinc oxide nanoparticle-capped catechin contents 1mg respectively presented a three phase release profile characterized by burst phase, lag phase and sustained phase it was observed in the release study that the initial burst release increases as the catechin content increased. In the first step of release which was caused by diffusion of the drug continued for 5 hours of incubation with a burst release of 0.6 mg. In the second phase, caused by drug diffusion and cleavage of the chains, catechin release was observed and in the final phase of catechin release, a near linear and continuous release was observed over 72-120 hours that reached 0.90 mg respectively in phase second and final phase. Thus it can be concluded that the catechin was encapsulated.

A study by Kailaku *et al.,* (2014) had reported that for nanoencapsulated catechin with chitosan, the drug release profile showed an apparent initial burst observed within the first 4 hours and exhibited the potential to release the loaded catechin sustainably.

Thus, the study suggests that, aside from the drug release profiles, there was an apparent initial burst within the first five hours of the produced zinc oxide nanoparticle-capped material demonstrating the potential to release the loaded catechin in a sustainable manner.

4.4.3.3. Results of Acetylcholinesterase inhibition by TLC

Studies on acetylcholinesterase inhibition using TLC showed that the acetylcholinesterase inhibition data of the autographic assay displays the catechin, synthesized zinc oxide nanoparticles and synthesized zinc oxide nanoparticle-capped catechin, with the Rf values being 0.63, 0.58 and 0.61 respectively.

The above observation recommends that the synthesized zinc oxide nanoparticle-capped catechin is a cholinesterase inhibitor.

4.4.3.4. Acetylcholinestrase inhibition activity of synthesized zinc oxide nanoparticle-capped catechin

The acetylcholinesterase inhibitory activity of the synthesized zinc oxide nanoparticle-capped catechin was studied.

Figure 40 illustrates the percentage of inhibition of acetylcholinesterase against a concentration range of synthesized zinc oxide nanoparticle-capped catechin. (0.75, 0.50, 0.25, 1, 1.25, 1.5 µg/ml).

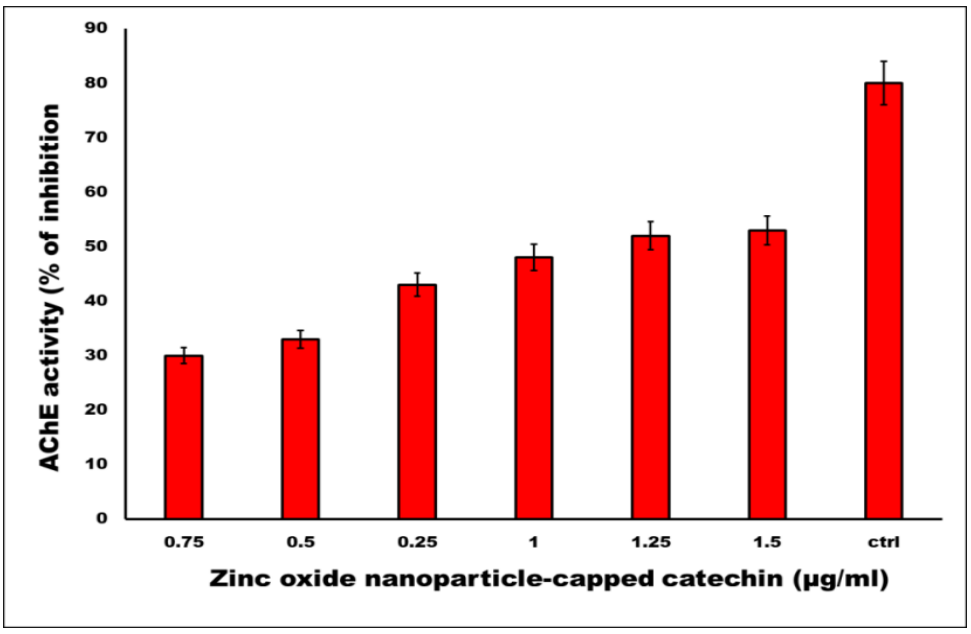

Figure 40: Acetylcholinesterase (AChE) inhibitory activity of synthesized zinc oxide nanoparticle-capped catechin

It can be assessed from the figure that the synthesized zinc oxide nanoparticle-capped catechin showed AChE inhibitory activity in a dose dependent manner with an IC_{50} value

increasing with extract concentrations. A concentration of 0.75 µg/ml followed by 0.5 µg/ml zinc oxide nanoparticle-capped catechin possessed 18 and 23 % low activity (< 30 % inhibition). The concentration of 0.25 and 1 µg/ml has shown 30 and 40% moderate activity (30-50 % inhibition). The concentration of 1.25 µg/ml has shown AChE inhibition activity of (> 50 % inhibition). A concentration of 1.50 µg/ml of the synthesized zinc oxide nanoparticle-capped catechin showed the highest AChE inhibition.

A similar kind of result was obtained by Ghareeb *et al.,* (2014) when he worked with a the plant extract from *Chlorella Vulgaris* (Green alga) which was a strong inhibitor of AChE activity and reported the lowest IC_{50} (40±2.3 µg/ml) value. Another study by Singh and Ramassamy, (2017), reported that AChE activity was reduced by 30 % at 12.50 µg/ml of *Withania somnifera* extract 50 % at 50 µg/ml of *Withania somnifera* extract. In another study, Ahmed *et al.,* (2010) stated that the individual compounds of curcuminoid mixture showed AChE inhibitory activity.

This result proved that the synthesized zinc oxide nanoparticle-capped catechin showed the highest AChE inhibition.

Hence it can be clearly seen from the results of Phase IV that the synthesized zinc oxide nanoparticle-capped catechin were had neuroprotective activity.

4.5. Phase V:

Assessment of *in vitro* neuroprotective activity of synthesized zinc oxide nanoparticle-capped catechin to neuro2a cells

This investigation was to study the *in vitro* neuroprotective activity of the synthesized zinc oxide nanoparticle capped catechin (ZnONPs-CAT) on neuro 2a cell lines. Cells which were a fast-growing mouse neuroblastoma line used to study neurodegenerative diseases were selected (van Der Laan *et al.,* 2019). Rivastigmine which is a cholinesterase inhibitor that inhibits acetylcholinesterase used to treat mild to moderate dementia, was also selected as the commercial drug and used as a standard. The *in vitro* neuroprotective activity of the synthesized zinc oxide nanoparticle-capped catechin was then studied using the MTT assay, Lactate Dehydrogenase (LDH) assay, Cell Morphology-DCFDA staining, SOD activity, AChE activity and Cell cycle analysis.

4.5.1. Results of Cell viability of neuro 2a cells using the synthesized zinc oxide nanoparticle-capped catechin

The toxic effect of the synthesized zinc oxide nanoparticle-capped catechin on neuro 2a cells studied by MTT assay after 24 hours treatment.

Figure 41 shows the *in vitro* cytotoxic effects of synthesized zinc oxide nanoparticle-capped catechin screened against neuroblastoma (neuro 2a) cell line.

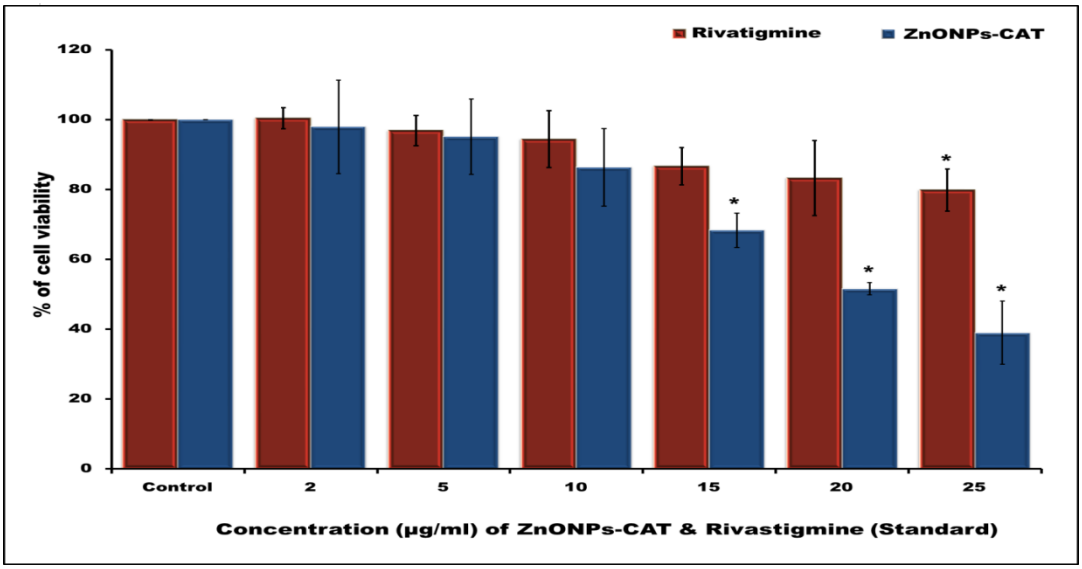

Figure 41: Effect of synthesized zinc oxide nanoparticle-capped catechin on cell viability in neuro 2a cells

Values are mean ±SD of triplicates * ($p < 0.05$)

It is revealed from the MTT assay as shown in the figure that with increase in concentration of rivastigmine and synthesized zinc oxide nanoparticle-capped catechin, there was a gradual decrease in the percentage of cell viability upto 10 µg/ml. However with further increase in concentration upto 25 µg/ml, there was a significant ($p<0.05$) decrease in the percentage of cell viability. Hence neuro 2a cells exhibited lower cytotoxicity; nevertheless, around 90 % cells were viable upon treatment with the lowest concentration of rivastigmine and synthesized zinc oxide nanoparticle-capped catechin. These low cytotoxicity effects suggest that synthesized zinc oxide nanoparticle-capped catechin are suitable for formulations of drug against neuronal disease.

The finding from this study that 90 % cells were viable upon treatment with the lowest concentration of rivastigmine and synthesized zinc oxide nanoparticle-capped catechin is supported by the work of Wang *et al*., (2016) who revealed that a new

multifunctional compound obtained by fusing donepezil (standard drug) with melatonin (compound of study) did not show significant effect on cell viability of neuroblastoma PC12 cells at 1-50 µm and these compounds were non-toxic.

It is thus revealed from the findings that, upto a concentration of 20 µg/ml of synthesized zinc oxide nanoparticle-capped catechin, there was no significant change in the percentage of cell viability (90 % cells are viable).

4.5.2. Results of Lactate Dehydrogenase leakage of synthesized zinc oxide nanoparticle-capped catechin

LDH inhibitors lower lactate production and decrease extracellular lactate indirectly lowering the production of signaling molecules involved in proliferation of cells .Cell membrane integrity and cytotoxicity of the synthesized zinc oxide nanoparticle-capped catechin was studied by determining lactate dehydrogenase leakage from neuro 2a neuroblastoma cell lines and finding out the integrity of the cell membrane to allow leakage of LDH.

Figure 42 indicates the effect of Lactate dehydrogenase on neuro 2a cells using synthesized zinc oxide nanoparticle -capped catechin.

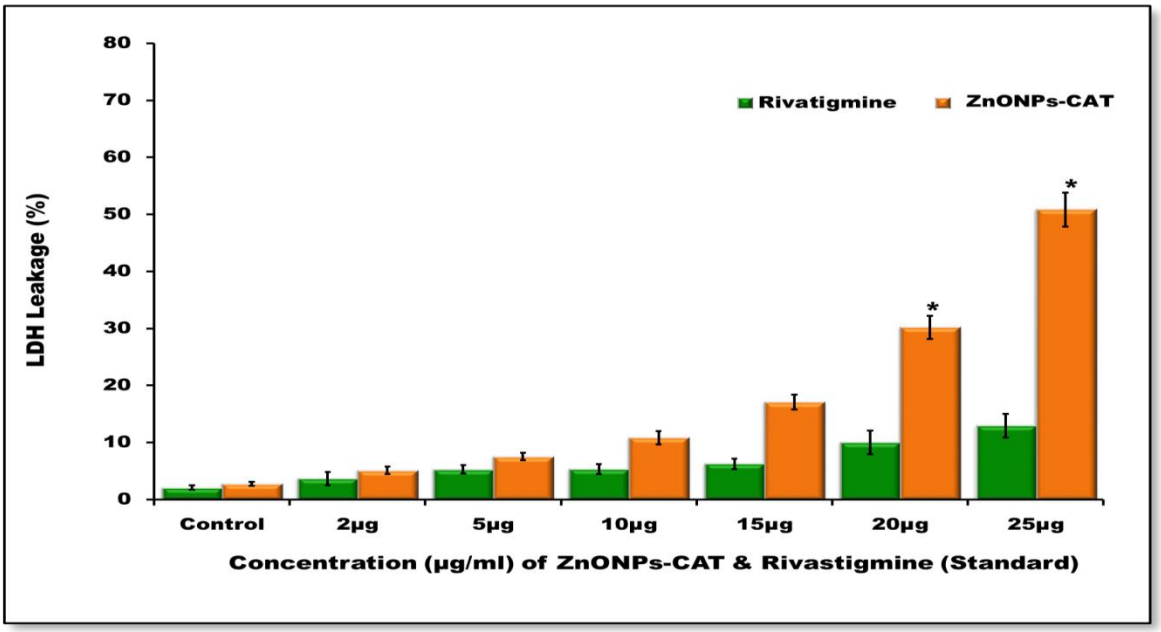

Figure 42: LDH leakage of synthesized zinc oxide nanoparticle-capped catechin

Values are mean ±SD of triplicates * $p < 0.05$

It is evident from the figure that the rivastigmine and synthesized zinc oxide nanoparticle-capped catechin treatment increased the LDH leakage from neuro 2a cells with increase in the concentration of rivastigmine and synthesized zinc oxide nanoparticle-capped catechin. To assess the toxicity of neuro 2a cells, the extracellular medium was used as a measure of membrane intensity. LDH was released into the culture media in a dose-dependent manner, demonstrating that the synthesized zinc oxide nanoparticle-capped catechin had less adverse effects upto a concentration of 15 µg/ml. Based on these findings, exposure to synthesized zinc oxide nanoparticle-capped catechin (2, 5, 10, 15, 20 and 25 µg/ml) for 24 hours did not inhibit cell proliferation.

The present study is o parr with a previous study conducted by Wiatrak and Balon, (2021), who reported that PC12 and THP-1 cell lines used as neuronal and microglia models in neurobiological research, showed the LDH leakage in a concentration dependent manner. In another study, Cacciatore *et al.*, (2021), reported that a compound (boron-based hybrid) acts as novel scaffolds for the development of drugs with neuroprotective properties and showed that the LDH activity of SH-SY5Ycells increased with increase in concentrations of the compound.

Hence the present results clearly indicate the results obtained in this test are no significant alteration in the percentage of LDH released was observed in the neuronal cells after synthesized zinc oxide nanoparticle-capped catechin expose at 24 hours time point.

4.5.3. Analysis of morphological changes in neuro 2a cell lines on treatment with synthesized zinc oxide nanoparticle-capped catechin

The synthesized zinc oxide nanoparticle-capped catechin and rivastigmine (standard drug) were used to observe morphological changes in the neuro 2a cell line under the microscopic.

Figure 43 shows the effect of synthesized zinc oxide nanoparticle-capped catechin on morphological characteristics of neuro 2a cell lines.

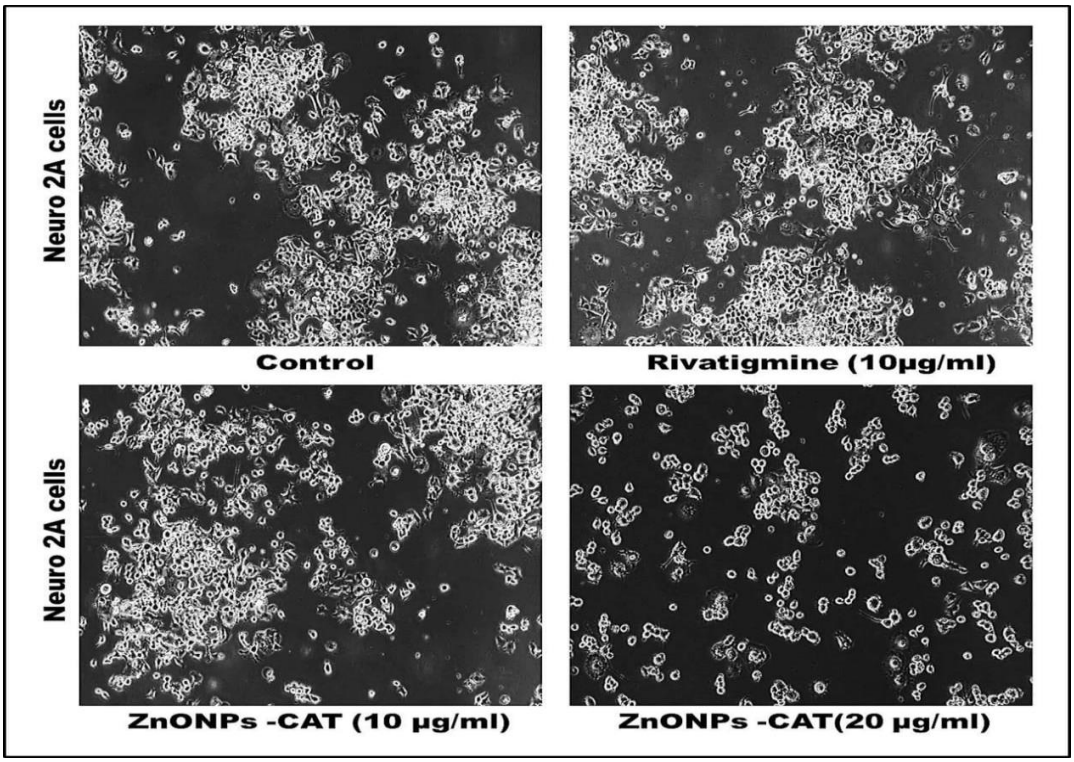

Figure 43: Microscopic images exhibiting the protective effect of synthesized zinc oxide nanoparticle-capped catechin toxicity against neuro 2a cell line

A) Control,

B) Cells were treated with rivastigmine (20 µg/ml) for 24 hrs treatment,

(C and D) Cells were treated with synthesized zinc oxide nanoparticle-capped catechin10 and 20 µg/ml) for 24 hrs.

It can be seen from the figure that a concentration of 10 µg/ml of synthesized zinc oxide nanoparticle-capped catechin resulted in more cell viability than 20 µg/ml of synthesized zinc oxide nanoparticle-capped catechin when compared to standard. This indicates that with increase in concentration of synthesized zinc oxide nanoparticle-capped catechin, the viability of cells decrease resulting in cell death. The increase in cell viability may owe to the synthesized zinc oxide nanoparticle-capped catechin having a great antioxidant potential to reduce the oxidative stress in neuro 2a cells. Further, the microscopic image confirmed that synthesized zinc oxide nanoparticle-capped catechin are non-toxic and can protect the neuro 2a cells against neurotoxicity.

Morphological changes by synthesized zinc oxide nanoparticle-capped catechin have also been reported in an earlier study by Boroumand *et al.*, (2015) who stated that morphological changes were induced by zinc oxide nanoparticles in leukaemia cells (WEHI-3 cells). Another study by Joshi and Rahman, (2015), stated that the apoptotic cells with

condensed chromatin and affected cell membrane, resulted in clumps of intense green fluorescent spots within the cells.

Thus it can be concluded from the above studies that the synthesized zinc oxide nanoparticle-capped catechin has a great antioxidant potential to reduce oxidative stress in neuro 2a cells.

4.5.4. Results of superoxide dismutase activity of synthesized zinc oxide nanoparticle-capped catechin

The cellular oxidative stress responses of the synthesized zinc oxide nanoparticle-capped catechin and rivastigmine (standard drug) against neuro 2a cell lines was studied by superoxide dismutase assay.

The effect of the synthesized zinc oxide nanoparticle-capped catechin on the superoxide dismutase activity of the neuro 2a cells is depicted in Figure 44.

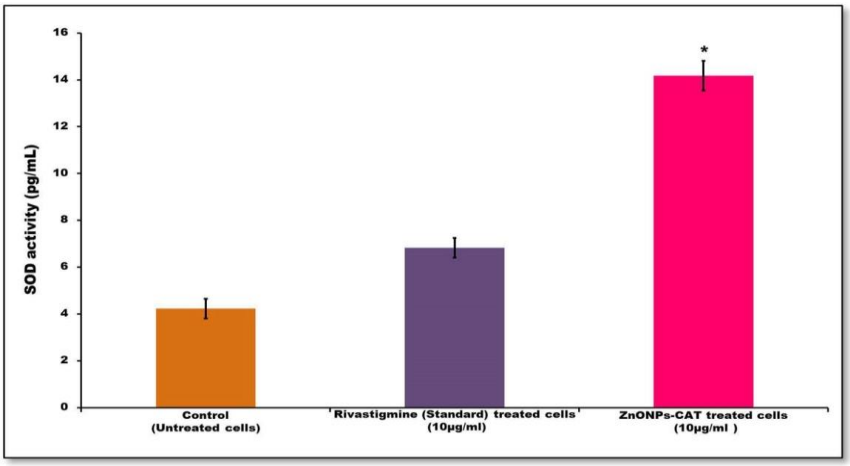

Figure 44: Effect of synthesized zinc oxide nanoparticle-capped catechin on SOD activity of the neuro 2a cells

Values are mean ±SD of triplicates * p <0.05

From the figure, it can be seen that the relative activity of SOD in the neuro 2a cells treated with rivastigmine for 24 hours was significantly higher than that of the control, whereas, in the case of the synthesized zinc oxide nanoparticle-capped catechin (10 µg/ml) treatment, an evident elevation of SOD activity was detected in the neuro 2a cells (13.9 pg/ml).

The presence of SOD activity in the synthesized zinc oxide nanoparticle-capped catechin in the present study is supported by a previous study by Law *et al.*, (2014) who

reported that an optimal concentration of *Escherichia coli* can induce intracellular ROS in SH-SY5Y cell lines to activate the expression of gene products.

Thus it can be inferred from the above that the relative activity of SOD in neuro 2a cells treated with synthesized zinc oxide nanoparticle-capped catechin for 24 hours was significantly higher than that of the control.

4.5.5. Results of DCFDA (DiChlorodihydro Fluorescein DiAcetate) staining of synthesized zinc oxide nanoparticle-capped catechin

Reactive oxygen species have been well-known to damage human tissues through protein oxidation and cross-linking, lipid peroxidation as well as DNA cleavage. To determine the potential effects of synthesized zinc oxide nanoparticle-capped catechin on oxidative stress, levels of ROS were measured using the fluorescent probe DCFH-DA in neuro 2a cell lines exposed to synthesized zinc oxide nanoparticle-capped catechin at 10 and 20 µg/ml for 24 hours.

Figure 45 depicts the effect of ROS generation in synthesized zinc oxide nanoparticle-capped catechin treated neuro 2a cells.

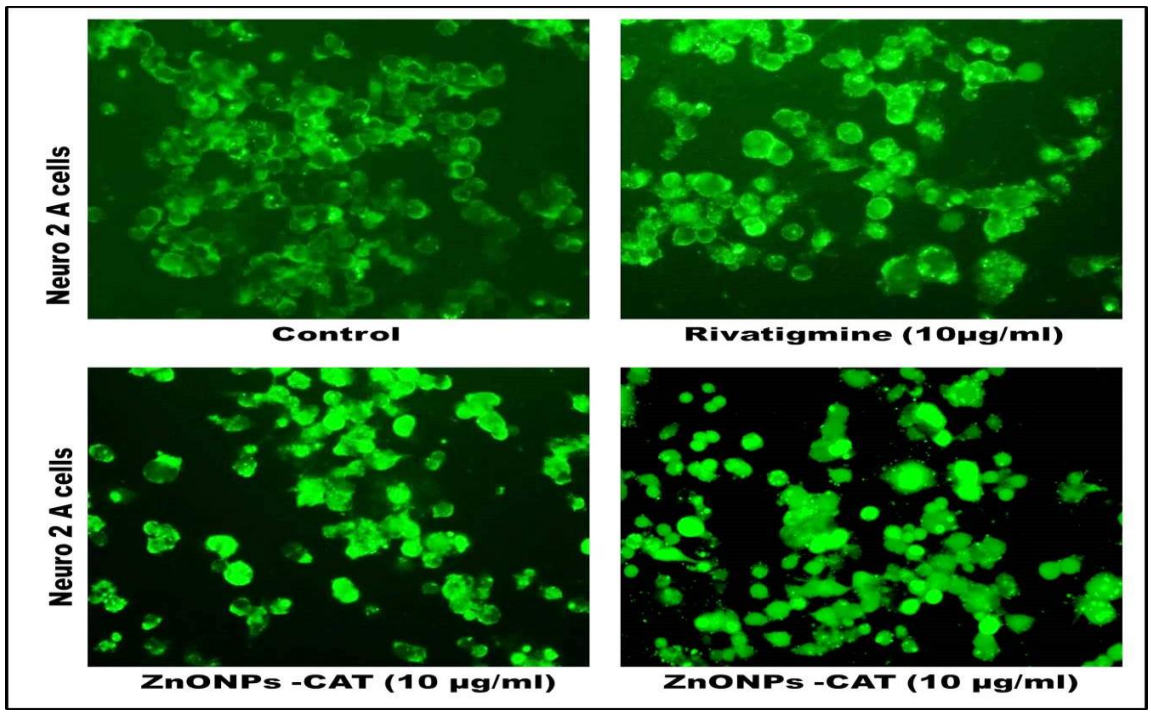

Figure 45: Effects of synthesized zinc oxide nanoparticle-capped catechin exposure on intracellular ROS levels.

Representative images of DCF staining of neuro 2a cells

It can be observed from the figure that the fluorescent intensity represents the level of ROS in neuro 2a cells. After treatment, the DCF fluorescence intensity was significantly increased in a dose-dependent manner in neuro 2a cell lines as shown in figure 45.. The DCF fluorescence intensity was much stronger in the cells exposed to synthesized zinc oxide nanoparticle-capped catechin (10 µg/ml) than the cells exposed to rivastigmine and synthesized zinc oxide nanoparticle-capped catechin (10 µg/ml). These data demonstrated that synthesized zinc oxide nanoparticle-capped catechin increased the production of intracellular ROS in a concentration dependent manner. Since the concentration of the synthesized zinc oxide nanoparticle-capped catechin was 10 µg/ml, it decreased the ROS damage in neuro 2a cell lines. As a result of this, the catalase activity, oxidizable substrates and iron binding capacity are normal.

The results of the present study are similar to the work of Guo *et al.* (2013), who stated that used rat retinal ganglion cells exposed to synthesized zinc oxide nanoparticle-capped catechin for 24, 42 and 72 hours, showed that the nanoparticles were taken up by the cells causing ROS increase which in turn cause increased expression of apoptosis markers.

The above finding confirms that the synthesized zinc oxide nanoparticle-capped catechin increased the production of intracellular ROS in a concentration dependent manner.

4.5.6. Results of Acetylcholinestrase activity of synthesized zinc oxide nanoparticle-capped catechin

The acetylcholinesterase inhibitory activity of the synthesized zinc oxide nanoparticle-capped catechin on neuro 2a cell lines was studied its understand neuroprotective activity .

Figure 46 illustrates the inhibition of acetylcholinesterase activity of the synthesized zinc oxide nanoparticle-capped catechin on treated neuro 2a cell lines.

From the below figure, it can be said that the zinc oxide nanoparticle-capped catechin when compared to the rivastigmine (standard drug), exhibited more than 85% acetylcholinesterase inhibitory activity at a concentarion of 10 µg/ml after 24-hours. This indicates that the synthesized zinc oxide nanoparticle-capped catechin can protect the cells from damage.

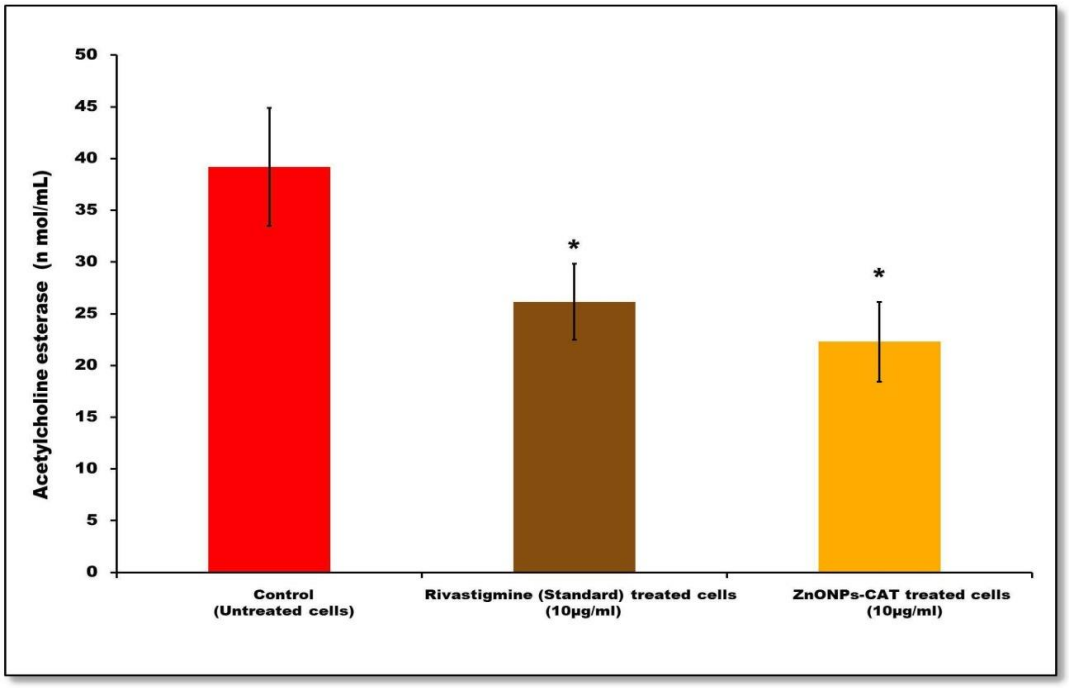

Figure 46: Inhibition of synthesized zinc oxide nanoparticle-capped catechin the acetylcholinesterase activity of neuro2a cells

Values are mean ±SD of triplicates * p <0.05

The above findings are in correlation with earlier reports. Rashed *et al.,* (2015) evaluated the neurological activity of the isolated compound from 80% methanol extract of *Ampelopsis brevipedunculata* aerial parts (peppervine). Another study by Feitosa *et al.,* (2011), stated that the acetylcholinesterase inhibitors from ethyl acetate and methanolic extracts of certain brazilian medicinal plants can be used successfully to treat symptoms of neurological diseases.

Thus this study evidenced that a concentration of 10 µg/ml of synthesized zinc oxide nanoparticle-capped catechin could inhibit acetylcholinesterase activity in neuro 2a cells.

4.5.7. Results of cell cycle analyses by Flow cytometer of synthesized zinc oxide nanoparticle-capped catechin

Understanding how therapies impact neuroblast proliferation and differentiation is made easier by evaluating the cell cycle of neuroblasts (Simoes *et al.,* 2021). Evaluating the effects of zinc oxide nanoparticle-capped catechin on neuroblast cell cycle phases can disclose its capacity to cause cell cycle arrest and enhance neuroprotection, providing

information on new treatment approaches to address neurodegenerative illnesses. Hence we evaluated the effects of the zinc oxide nanoparticle-capped catechin on cell cycle progression in neuro 2a cells. The findings showed that treatment with zinc oxide nanoparticle-capped catechin significantly reduced the number of cells in the G0-G1 phase, which may indicate increased cell proliferation and cell cycle progression. This could imply enhanced neurogenesis and potential neuroprotective effects which are beneficial in the context of neurodegenerative diseases.

The neuroblastoma (neuro 2a) cells were treated with the zinc oxide nanoparticle-capped catechin and also rivastigmine (standard drug) to study the different phases of the cell cycle (G0/G1, S and G2/M phases).

Figure 47 depicts the results of cell cycle analysis

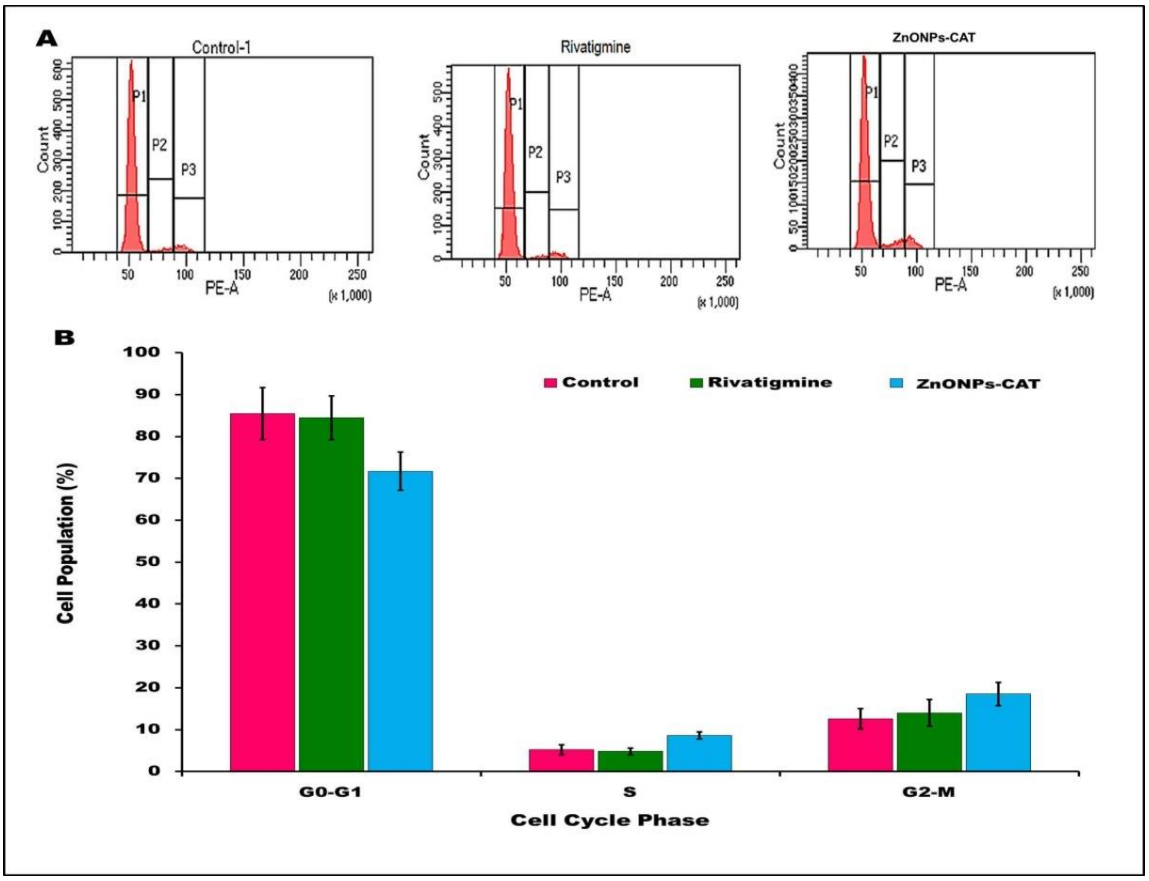

Figure 47: Cell cycle analysis by flow cytometer

A) Cell cycle analysis and

B) Quantification was performed using flow cytometry following staining with propidium iodide staining in neuro 2a cells.

It is understood from the figure that there were significant alterations in cell cycle of the neuro 2a after 24 hours pertaining to decrease in the percentage of cells in G0/G1 and G2/ M phases and an increase in the percentage of cells in S phase. Besides significant dose response relationship were found in phases G2/ M ($18.5<P<0.1$). Thus it can inferred that cell cycle dysregulation has been involved in the quiescent state of the cell cycle analysis. The proliferation in most of the cells were arrested in the G0/G1 phase. Mature senescent and differentiated cells were also present in the G0 phase.

The finding that the proliferation in most of the cells were arrested in the G0/G1 phase as reported in the present study is in accordance with the study of Paramasivam *et al.*, (2015) who stated that thymoquinone treated neuro-2a cells were arrested in the G2/M phase of cell-cycle.

Thus it clearly indicates that the significant dose response relationship was found in phases G2/ M.

From the overall outcome of Phase V, in can be concluded that cell cycle dysregulation was involved in the quiescent state of the cell cycle of neuro 2a cells.

Highlights of the findings

- Based on docking studies, a catechin-rich plant, namely, *Camellia sinensis* was selected.
- The leaves of *Camellia sinensis* were found to contain a good amount of antioxidants and radical scavenging activity. The main active component catechin was isolated and characterized.
- The zinc oxide nanoparticles synthesised from *Camellia sinensis* leaf extract were characterized and found to be a good source of antioxidants with acetylcholinesterase inhibitory activity.
- Synthesized zinc oxide nanoparticle-capped with catechin had neuroprotective activity.
- The effect of synthesized zinc oxide nanoparticle-capped catechin on neuro 2a cells showed less toxicity, arrest of cells in quiescent state, antioxidant activity and acetylcholinesterase activity.

An outline of the findings of the present study and conclusions drawn thereof are presented in the following chapter.